UNIVERSITÀ DEL PIEMONTE ORIENTALE

SCHOOL OF MEDICINE

Department of Health Sciences

Master's Degree in Medical Biotechnology

A step forward in understanding Human Cytomegalovirus infection: the induction of paracrine senescence in renal epithelial cells

TUTOR:
Professor Marco De Andrea

CO-TUTOR:
Raviola Stefano, PhD
Caneparo Valeria, PhD

Candidate: **Federica Castiglioni**
Matricula Number: **20028389**

Academic Year

2023/2024

INDEX

SUMMARY

Rational of the study: Human cytomegalovirus (HCMV) is a widespread β-herpesvirus, and the major infectious cause of birth defects as well as an important opportunistic pathogen. Active HCMV infection is associated with poor graft outcomes; however, the underlying pathogenic mechanisms remain inadequately understood. Given that the accumulation of senescent cells has been identified as a principal driver of renal fibrosis and poor transplant outcomes, this experimental thesis aims to establish a renal infection model to evaluate the pathogenic mechanisms linked to HCMV-induced paracrine senescence.

Planning of the study: Renal proximal tubular epithelial cells (RPTECs) were infected with HCMV TR strain. Transcriptomic and multiplex immunoassay analysis were used to evaluate the overall cellular response to HCMV. Then, SA-β-gal staining, EdU proliferation assay, secretome studies and microscopy analysis were performed to characterise the paracrine senescence phenotype studies. Finally, we evaluated the contribution of IL-6 to this signature of senescence.

Results: We demonstrated that RPTECs were fully permissive to HCMV infection. Moreover, the transcriptomic profile of HCMV-infected RPTECs underlined a strong antiviral and pro-inflammatory response, which was corroborated by a significant release of pro-inflammatory molecules through multiplex immunoassay analysis. Intriguingly, many molecules induced upon infection are included in the senescence-associated secretory phenotype (SASP). In parallel, ELISA experiments demonstrated the upregulation of markers of renal tubular injury such as NGAL. Interestingly, Gene Set Enrichment Analysis (GSEA) revealed hallmark of allograft rejection during infection, paralleled by a strong release of IP-10 and RANTES which are strongly associated with kidney graft dysfunction and rejection. Consistently, infected RPTECs showed an upregulated β-galactosidase activity, and a decreased proliferation rate with the release of a massive amount of inflammatory cytokines. Microscopic analysis data revealed signs of paracrine senescence in cells adjacent to the infection sites. Specifically, there was an induction of senescence dependent on the action of IL-6. This finding was confirmed by data obtained from experiments conducted with conditioned media from previous infections and the use of an IL-6R inhibitor.

Conclusions: RPTECs represent a reliable model of infection, fully supporting HCMV replication *in vitro*. HCMV induces a senescence-like phenotype in primary kidney proximal

tubular epithelial cells, suggesting an association with renal ageing and disease progression, as observed in the course of kidney transplant failure and rejection.

1. INTRODUCTION

1.1 Human Cytomegalovirus

1.1.1 Human Cytomegalovirus: General Features

Herpesvirus (HVs) is a large family of invasive and wide-spread pathogens able to infect mammalian and other species characterized by the ability to establish latency. Human Cytomegalovirus (HCVM), also known as human herpesvirus 5 (HHV-5), belongs to Herpes virus family. The HVs are large-DNA viruses characterized by packed-DNA in an icosahedral capsid. It became apparent from sequence-based comparisons that mammalian and avian HVs were descended from a common ancestor and that the three taxonomic subfamilies corresponded to major distinct lineages[1]. Based on biological criteria it has been possible to classify the HVs into three different subfamilies: Alpha-, Beta-, and Gamma-herpesvirus. The most important Alpha-herpesvirus are Herpes simplex virus types 1 and 2 and varicella-zoster virus (HSV-1, HSV-2 and VZV) that infect primarily nervous system cells causing latency. Human Cytomegalovirus is one of the main Beta-herpesvirus with human herpesvirus 6 and 7 (HHV-6 and HHV-7). Kaposi's sarcoma-associated herpesvirus (KSHV) and Epstein-Barr virus (EBV) are the two most common members of the Gamma-herpesvirus which main peculiarity is the ability to induce latency into the lymphocytes.

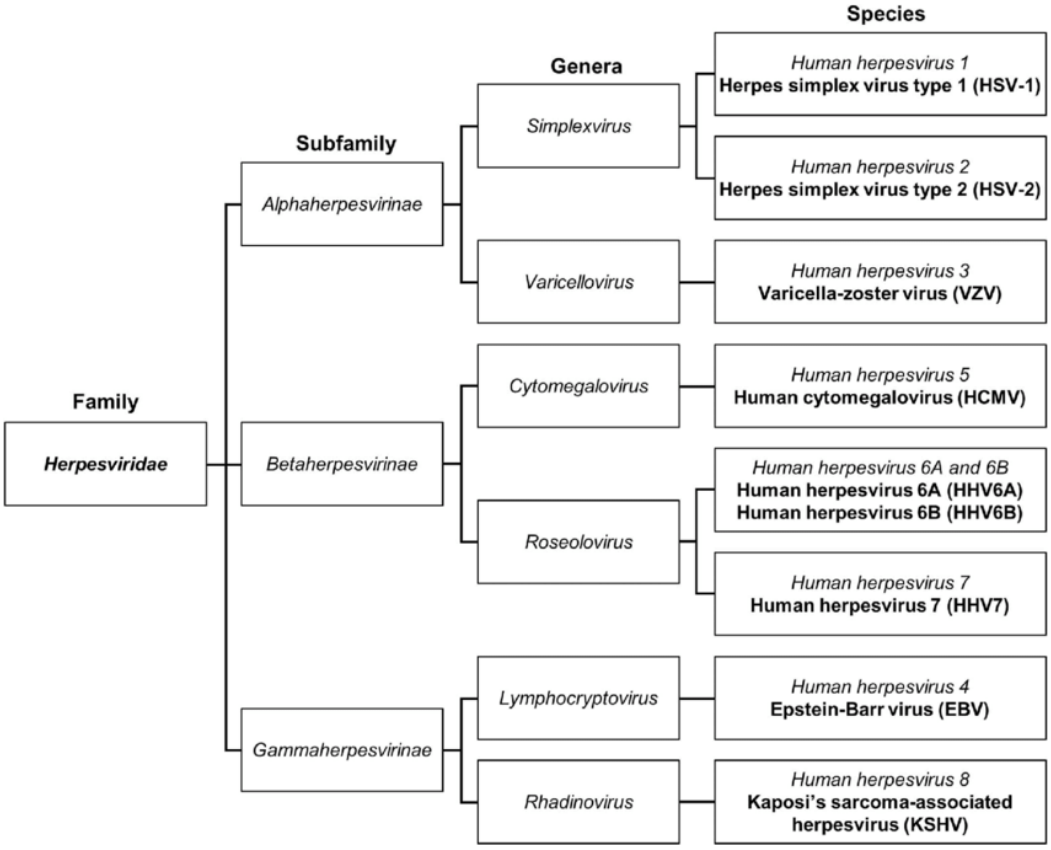

Figure 1. ***Taxonomy of the Herpesviridae family based on phylogenetic analysis of whole viral genomes. (Chodosh, 2020)***

HCMV is characterized by a double-stranded linear DNA genome ranging between 196 and 241 thousand base pairs[2]. This is the largest virus genome belonging to the Beta-Herpesvirus family: it encodes for 160 gene products plus multiple non-canonical transcripts, and it is reinforced by mechanisms of non-canonical translation. The HVs genome is divided into "core genes" and "non-core genes". The first ones are maintained among all the different subfamilies; instead, the "non-core" genes are involved in the replication and life cycle of the virus. The HCMV proteins are distinguished in immediate-early (IE), early (E), and late (L) and their expression is due to a series of events starting from the transcription of IE that are essential.

The immune fitness of the patient is determinant to establish the type of HCMV infection. Usually, immunocompetent individuals do not display any symptoms of infection. Nevertheless, it may also present a nonspecific febrile illness, or an infectious mononucleosis-like syndrome characterized by fever, lymphadenopathy, and lymphocytosis. The real problem is the HCMV ability to establish latency in peripheral blood monocytes, epithelial and endothelial cells. On the other hand, if the individual is immunocompromised, such as organ-transplant recipients or acquired immunodeficiency syndrome (AIDS) subjects, the HCMV has

a high ratio of mortality and morbidity. Solid-Organ Transplant Recipients can develop primary CMV infection if they receive an allograft from a CMV-seropositive donor; or secondary if the recipient got a reactivation because of the stress of the procedure[3].

CMV infection during pregnancy can lead to intrauterine foetal infection and congenital CMV disease[4]. Vertical transmission of CMV from mother to foetus is quite diffuse globally. This type of infection can lead to severe consequences such as hearing loss, birth defects and neurodevelopment complications.

Technically, CMV infection is mainly due to the exposure to body fluids of CMV-seropositive individuals. In particular, during childhood, the infection is spread through breast milk, saliva, and urine; instead, during adult life through semen and vaginal secretion. HCMV is globally spread that about 90% of people are simultaneously seropositive for at least one or two herpesviruses[5].

1.1.2 HCMV Virion Structure

All the different herpes viruses have a similar structure. Indeed, they are all characterized by a doublestrand linear DNA containing cis-acting sequence for packaging process during the replication. The DNA is packed in an icosahedral nucleocapsid, rolled up by a tegument layer, to finish with the envelope which is the one that confer the typical spherical shape to the virion. The envelope surface is characterized by the glycoprotein complex used to recognize the cellular molecules through which bind and infect cells. This typical conformation is shared through the entire herpes family.

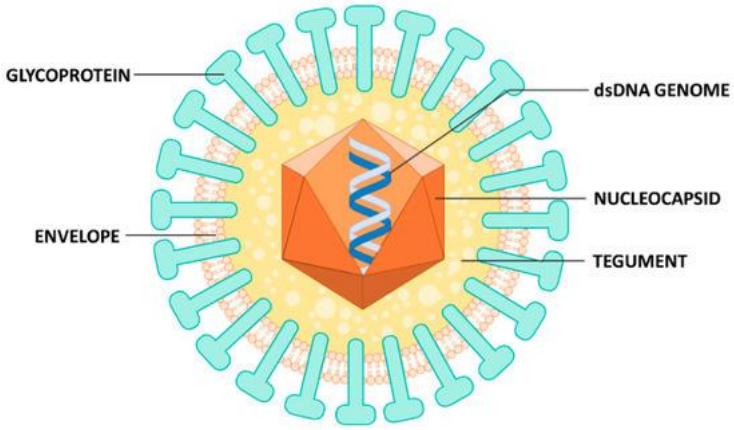

Figure 2. ***Structure of HCMV virion. (Gugliesi, 2020)***

Electron cryomicroscopy analysis revealed that the capsid is composed of 150 hexamers and 16 pentamers to make the icosahedral structure. Herpesvirus capsid assembly and viral DNA

packaging takes place in the nucleus of infected cells and is dependent on the virus scaffolding proteins[6]. Furthermore, the infected cells are able to release complete nucleocapsid with packed DNA inside, but also empty structures, known as dense bodies, that are the most abundant. HCMV is characterized by the major capsid proteins composed of the minor capsid protein-binding protein and the minor capsid protein and the small capsid protein. This triplex structure brings together exons and pentamers.

In HCMV, tegument is not completely attached to the capsid. There is a protein layer between the lipid envelope[7] and the capsid itself. It is known that tegument proteins are involved in the transport of the nucleocapsid with the viral genome inside the cellular nucleus. This mechanism happens through the action of UL47 and UL48 that collaborate with the microtubule motor proteins to facilitate the delivery of the viral genome. pp71 is an essential HCMV protein localized on the tegument layer. In fact, this protein is a trans-activator involved in the IE promoter activation after the viral entry into the infected cells[8]. pp65 and pp150 are the two most abundant proteins that characterise the tegument layer. pp150 is involved in the viral entry and recent studies have demonstrated that the expression of this gene is essential for productive HCMV replication. pp65 is delivered to the nucleus of permissive cells at the very start of a lytic infection[9]. pp65 mediates both innate and adaptive immune response and it is involved in the IE1 phosphorylation avoiding the presentation on the MHC class I. It is also involved in the protection of the infected cells inhibiting natural killer activity. During the early time-point of the infection, it is possible to detect either pp65 and pp150 in the nucleus; then, they translocate to the cytoplasm. pp28 is the last tegument protein. It is quite immunogenic and characterized by a myristylation site that allows the association with cellular and virion membranes; in fact, it is involved in the formation of viral particles and their egress.

The HCMV lipid bilayer envelope is characterized by different glycoprotein involved in the entry of the virions inside the target cells. In particular, the cellular tropism of the virus is due to the glycoprotein complexes that characterise the virion surface and are able to interact with specific cellular structures. The adaptative immune system will produce specific antibodies able to recognize the Glycoprotein complex III in order to avoid the entry of the virion.

1.1.3 HCMV binding, entry and replication

Virus attachment and penetration are rapid and efficient in both permissive and non-permissive cell types. In permissive cells, herpesviruses infection can lead to two different outcomes: latent and lytic cycle. However, since productive replication is observed in very restricted range of human cells, a post- penetration block to viral gene expression is thought to restrict replication

in non-permissive cells[10]. The mechanism of infection is conserved in the entire family of herpesvirus, but the combination of the glycoprotein can be different depending on the target cell. The fusion machinery conserved among the herpesvirus family is the heterodimer gH-gL and the fusion glycoprotein gB[11].

HCMV is characterized by two different structures, the trimer and the pentamer, that are differentially used by the virions depending on the cells they will infect. The trimeric complex is composed of gH-gL and gO and it is used by the virions for fibroblast. The pentameric complex, instead, is characterized of gH-gL plus UL128, UL130, UL131A and it will allow to entry in the endothelial and epithelial cells. These two complexes recognize different receptors: the trimer is able to bind to platelet-derived growth factor receptor α (PDGFRα); instead, the pentamer recognize the neuropilin-2 (Nrp2) to mediate the entry in the cells. The entry mechanism is quite different between these two complexes. In fact, the trimer will cause the fusion of the viral membrane with the cellular one and this does not affect the pH. Instead, the pentamer will cause the endocytosis of the virion in the cell and this is possible because of the change of the pH[12].

After the binding with the receptor and the effective entry in the cell, the nucleocapsid is brought to the nucleus where the viral DNA is injected. During the immediate-early time point of infection it is possible to detect the tegument protein pp65 in the nucleus: this will translocate in the cytoplasm during the replication.

In presence of lytic cycle, the major immediate early locus (MIE) starts to be expressed one hour post infection. In fact, this locus is characterized by the immediate early (IE) genes, such as IE1 and IE2, that acts as trans-activators and auto-simulators of viral genes. This complex will allow the transcription of the Early genes that are essential for the viral replication. E genes encode mostly non-structural proteins, including viral DNA replication factors, repair enzymes, and proteins involved in immune evasion[13]. These genes are essential to transcribe Late genes, which encode for structural proteins and are essential for virion packaging, during viral genome replication. The new synthesis of viral genome starts 16 hours after infection, and it occurs in the cell's nucleus with the packaging process. It has been demonstrated that CMV is not able to encode deoxyribonucleotide biosynthetic enzymes, thus, the virus must depend on the host cell metabolism to ensure a sufficient supply of dNTPs for its DNA replication[14]. Because of this viral necessity, the infection will induce an S phase-like state: the cells fail to undergo cellular DNA replication and division as a result of block in cell cycle progression that prevent the host DNA replication machinery from competing with the virus for access to DNA precursors [15].

The assembly of the nucleocapsid will occurs in the nucleus and it will also obtain a temporary envelope from the nuclear membrane. The nucleocapsid will reach the cytoplasm through the vesicle-mediated transport and there it will obtain the tegument layer. The final envelope is due to the Golgi apparatus. When the virion is mature, Golgi's vesicles will bring the new-formed virions to the cellular membrane, and they will be released to the extracellular environment after fusion of the membranes.

In contrast, latent infection[13] is determined by the regulation of the viral major immediate early promoter (MIEP). Particularly, the down-regulation of MIEP through epigenetic modifications and the presence of the viral transcript LUNA are essential to induce the expression of latency genes[16]. Indeed, it has been demonstrated that a reduction of LUNA transcript influences the expression of the correlate genes. The expression of these genes allows the viral genomes to remain in the nucleus in a quiescent state until the reactivation due to stressful stimuli and immunosuppression conditions, such as those to prevent rejection of transplanted organ. Essentially, the virus infects the cells and then it induces the transcription of latency-associated genes instead of producing new effective virions.

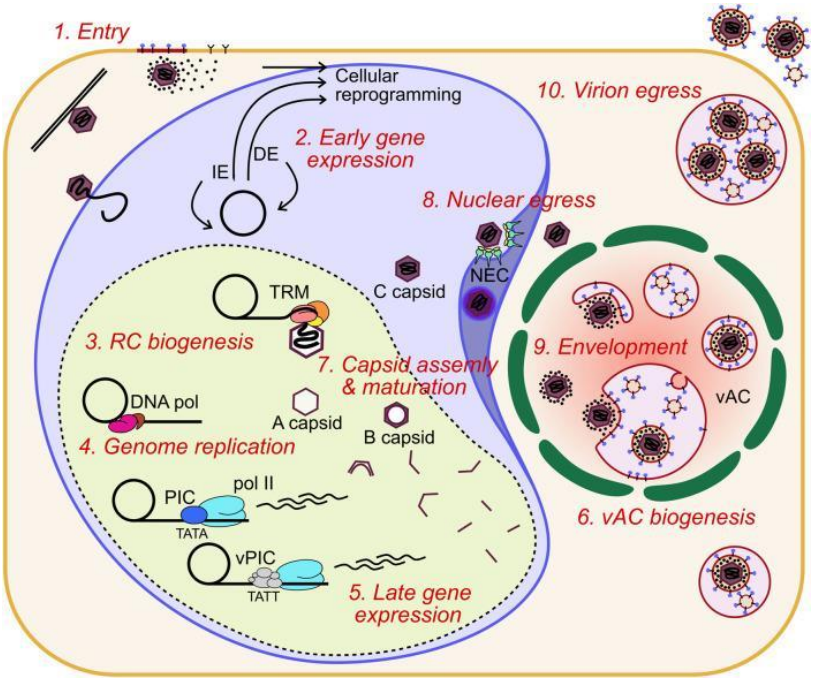

Figure 3. ***HCMV lytic replication cycle. (Turner, 2022)***

1.1.4 Tropism and transmission of HCMV

HMCV transmission in human has been distinguished in two different mechanisms: vertical and horizontal. The vertical transmission takes place during birth through placenta, vaginal secretion and then breast milk. Nevertheless, the horizontal transmission is the most common

and it happens because of direct contact with body fluids, or blood transfusion and organ transplant such as lung and kidney. The most common transmission is oral-dependent, also because the epithelial cells of the upper respiratory tract have an elevated susceptibility to infection.

Usually, the HCMV primary infection occurs in the epithelium of the upper alimentary, respiratory, or genitourinary tracts[17]. The infection spreads mainly through a mechanism cell-mediated to reach secondary organs; the alternative is through cell-free viruses. If infection occurs in endothelial cells, they can transfer the infection to secondary sites. In addition, the virus tends to recruit cells of innate immunity, such as monocytes, because as well as support the replicative cycle of the virus itself, they are excellent for transmission throughout the organism. Furthermore, monocytes and CD34+ cells are an important site of latency.

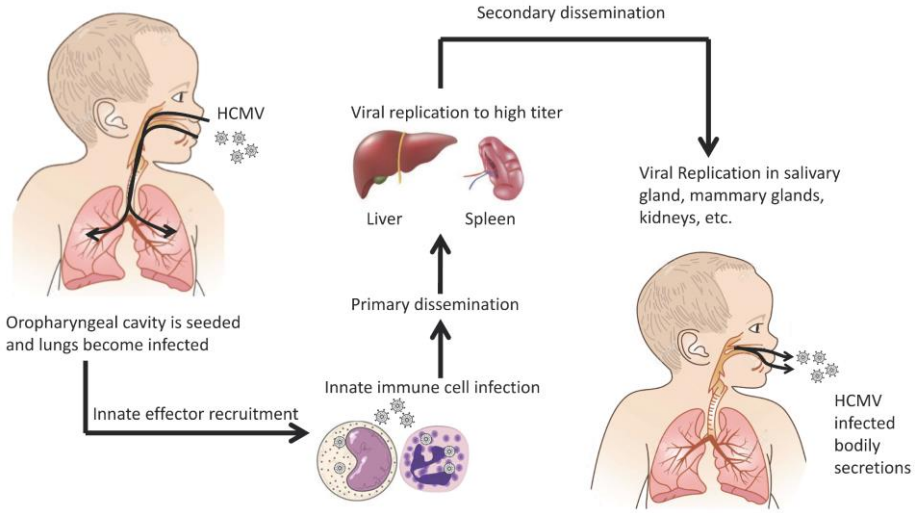

Figure 4. ***Overview of human cytomegalovirus (HCMV) dissemination. (Jackson, 2018)***

As mentioned before, after solid organ transplant (SOT), one of the leading causes of mortality and morbidity is HCMV infection; in fact, it is one of the most common pathogens. Patients at the highest risk are the seronegative ones which receive an organ from HCMV-seropositive patients because they lack of the adequate immune adaptative response. HCMV-seropositive patients can either manifest reactivation or infection up to 20% of the cases. HCMV is still the most important viral pathogen after kidney transplantation[18]. The infection can manifest as CMV syndrome, characterized by fever, atypical lymphocytosis, neutropenia or thrombocytopenia, and malaise, or as tissue-invasive disease[18,19]. Early CMV disease was found to increase the risk of cardiovascular mortality beyond 100 days posttransplant, whereas asymptomatic infection did not reach statistical significance.

1.2 Senescence

1.2.1 Cellular senescence: definition and classification

Cellular senescence is a cell state triggered by stressful insults and certain physiological processes, characterized by a prolonged and generally irreversible cell-cycle arrest with secretory features, macromolecular damage, and altered metabolism[20]. In fact, senescence is different from quiescent state because of the inability of the cell to return to proliferate in presence of the correct stimuli. Hayflick and Moorhead [21] correlated the cellular senescence to the finite replicative lifespan of the cells due to the telomere shortening. This is also the reason why senescence has been linked to aging: the cells lose their ability to proliferate and to replace the damage ones provoking an accumulation in the aged tissue. However, despite the hypoproliferative feature, the senescent cells are still metabolically active and capable to perform the functions of the replicative-competent cells.

Several stressors can induce a senescent state, including DNA damage, telomere dysfunction, oxidative stress, endoplasmic reticulum (ER) stress, chromatin alteration, mitochondrial malfunction, and other factors. Senescence has been classified on the base of the stimuli that induce the state and the respective effects[21]. We can distinguish four different types of senescence-induced mechanism:

i) Replicative senescence is the state in which the cells have reached an irreversible cycle arrest following multiple rounds of replication. This condition happens when the telomere, region that prevent the loss of genes during the replication of the cells, become too short[22].

ii) Oncogene-induced senescence (OIS) is an anti-tumour mechanism upon activation of oncogene such as p53 and RAS[23].

iii) Genotoxic-induced senescence (GS) is the consequence of the exposure of cells to mitogenic oncogenes or genotoxic treatment such as radiation or chemotherapy: if significant genotoxic stress exceeds the repair capacity, the cells enter in a senescence state to avoid the spread of the damage.

iv) Developmental and tissue repair senescence is a paracrine phenomenon due to the release of proinflammatory interleukins, chemokines, cytokines, matrix metalloproteinases and growth factors, known as senescence-associated secretory phenotype (SASP), by the senescent cells. This mechanism is typical of non-disease contexts and it supports embryogenesis, development, and tissue regeneration[24].

1.2.2 Hallmarks of senescence

Due to the different types and meaning of senescence there are not unequivocable markers to identify senescent cells in an *in vivo* or *in vitro* context. Essentially, one single marker is not sufficient to declare a senescent status, but we need a combination of these. The stimuli cited before have a consequence on the morphology of the cells; especially senescent cells are characterized by irregular cell shape due to the alteration of the cytoskeleton, enlarged cytoplasm and alteration of the plasma and nuclear membrane. Since senescence is essentially characterized by an irreversible cell cycle arrest, we can distinguish four main hallmarks useful to determine a senescent profile[25]: i) the retinoblastoma family proteins; ii) p53; iii) CDK2 inhibitor $p21^{WAF1/Cip1}$ (CDKN1A), and iv) CDK4/6 inhibitor $p16^{INK4A}$ (CDKN2A). Senescent cells have an accumulation of all these proteins, and they are mainly induced by the DNA damage response (DDR). These proteins are responsible for the activation of RB family proteins and consequent inhibition of E2F transactivation which is necessary for cell-cycle progression. This overexpression is due to inflammatory cytokines and release of reactive oxygen species (ROS). These features are typical of other forms of cell-cycle arrest not senescence-dependent. In fact, p16, one of the main senescence markers, is expressed also in other circumstances not related to ageing.

Senescent and ageing cells are characterized by mitochondrial disfunctions. In particular, the main features are an increased mitochondrial mass and DNA content that will compensate the disfunction of the mitochondria itself and the decreased mitochondrial membrane potential (MMP). This last feature is related to ROS production and proton leak that can affect the electron transport chain (ETC). The increase in ROS release is also related to the DNA damage. All these characteristics result in a decrease mitochondrial ATP production, indeed senescent state was linked to an increase in ADP and AMP production[26]. This increased ratio leads to the activation of AMP-activated protein kinase (AMPK) that in turn activates p53 increasing the expression of p21 which is involved in cell-cycle arrest. Furthermore, different studies[27] highlighted an increased glycolysis in senescent fibroblast suggesting a metabolic shift in these cells. p53 is involved also in this mechanism of the senescent state. In fact, it regulates the glycolysis antagonizing the glucose uptake by inhibiting the expression of the transporters GLUT1 and GLUT4. Furthermore, p53 is involved in the conversion of glucose to pyruvate slowing this rate and promoting a senescent status.

Lysosomes are membrane-bound intracellular organelles with a relevant role in metabolism and in organelle and protein quality control[28]. It has long been known that the lysosomal

compartment is largely expanded in senescent cells and that they increase also in number in these cells. In fact, the increased lysosomal mass has been linked to senescence-associated beta-galactosidase (SA-β-gal) activity, one of the markers for the evaluation of this status. Another possible marker related to the lysosome is the accumulation of lipofuscin in the lysosome itself. From the macromolecular point of view, the main features of the senescent cells are the shortening of the telomeres and persistent DNA damage. One of the most common form of DNA damage, termed telomere-associated foci (TAFs), can exist at telomeres due to oxidative DNA damage at telomeric G-reach repeats, irrespective of telomere length or sheltering loss[29]. Senescent cells are also characterized by permanent DNA damage foci defined DNA-SCARSs: DNA segments with chromatin alterations reinforcing senescence; these structures are involved in SASP regulation. Histone γH2AX is the most sensitive marker of double-stranded DNA breaks (DSBs) and telomere shortening[30]: when activated it is phosphorylated at the C-terminal serine-139. In damaged cells there is an accumulation of phosphorylated histone γH2AX and this accumulation induces a p-53-dependenct cellular arrest.

One of the changes that characterise the senescent cells is the secretome that is called senescence associated secretory phenotype (SASP)[25] because of its composition and involvement. Especially, it is characterized mainly by pro-inflammatory cytokines, chemokines, growth factors, angiogenic factors, proteases, bioactive lipides, matrix metalloprotease. It is not known the exact composition of the SASP and this can change through different cell lines; cells themselves and different stimuli can influence the composition of SASP. The main idea is the presence of key players in the SASP able to mediate a paracrine effect in the neighbouring cells and to cause the pathophysiological effects of senescent cells. Many members of the SASP are produced as soluble factors regulated by transcription factors and directly released by the cells or they can be transmembrane protein released later. The main activator of these classical SASP is DNA damage through NF-kB, but there is also the non-canonical DNA damage response mediated by p38MAPK and the activation of the inflammasome through IL-1 and IL-6. SASP have a crucial role in the removal of senescent cells from the tissue guaranteeing the homeostasis of the tissue itself. This role is possible due to the activation of the immune system by the SASP themselves. This secretory phenotype is also involved in wound healing, tissue plasticity, persistent chronic inflammation, and in angiogenesis and metastasis in tumorigenic context.

Senescent cells release a higher content of extracellular vesicles (evSASP) compared to proliferating cells. These evSASP are enriched of interferon-related proteins, antiapoptotic proteins, several mi-RNA and they can induce paracrine senescence in healthy cells.

Interestingly, metabolite regulators have also been found inside evSASP conferring them intrinsic metabolic activity[31]; these metabolites can also regulate the SASP. Overall, it is not yet exactly defined the SASP composition, and the biological variation may have an impact on the senescence-based molecular signatures.

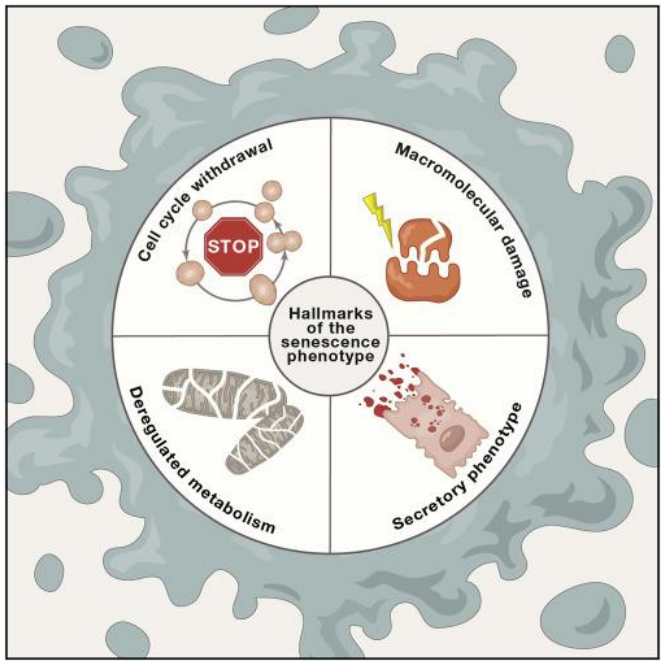

Figure 5. ***The hallmarks of the senescence phenotype. (Gourgulis, 2018)***

1.2.3 Senescence and chronic kidney disease (CDK)

Acutely senescent cells are widely recognized as performing key physiological functions *in vivo* promoting normal organogenesis, successful wound repair, and cancer defence[32]. In this situation the senescent cells are involved in embryonic organogenesis and tissue homeostasis; they are removed by leukocytes and natural killer after their contribute. However, an accumulation of senescent cells in response to stressors contributes to organ dysfunction, fibrosis and ageing. This "chronic" condition leads to proinflammatory environment favourable for different diseases.

Older and injured kidney shows an increased susceptibility to acute kidney injury (AKI) that can turn in chronic kidney disease (CKD) with progressive renal fibrosis. Senescent cells are accumulate in the kidney in three broad settings: with age, with any insult causing acute kidney injury, including post-transplantation, and in chronic kidney disease[33].

The upregulation of NF-κB, tumour growth factor beta (TGF-β) and hypoxia-inducible factor (HIF) affect tubule epithelial cell proliferation, cellular apoptosis and EMT. These phenomena are associated with senescence in tubule epithelial cells which is the primary location for renal

senescence and kidney failure in general. Interestingly, in human renal transplant biopsies, a series of patients with glomerular disease were characterized by p16 staining in glomerular, tubular and interstitial cell nuclei. The positive staining was also present in podocytes, parietal epithelium of glomeruli, vascular smooth muscle cells, and interstitial cells. Human studies have linked pre-transplant senescent cells in the kidney to the development of interstitial fibrosis, tubular atrophy, and chronic allograft nephropathy, as well as elevated mRNA expression of $p21^{CIP1}$ and $p16^{INK4a}$, which are associated with poor outcomes.

1.2.4 Evidence of viral induced senescence

Viruses represent an underrated type of stress involved in cellular senescence, however the relationship between virus and cellular senescence is proved to be very complex. This is one of the mechanisms, together with apoptosis and autophagy, used by the organism to protect itself. Virus-induced senescence (VIS) is indistinguishable from other forms of cellular senescence and is accompanied by a senescence-associated secretory phenotype (SASP), which comprises pro-inflammatory cytokines, extracellular-matrix-active factors and pro-coagulatory mediators[34]. This phenomenon is related to different types of virus and cellular lines, and it is not necessary that the cell is permissive to the viral replication.

The main connection between virus and senescence is the activation of the cGAs-STING pathway, which are viral genome sensor that induce the transcription of the type I interferons and the pro-inflammatory molecules. It has been demonstrated the crucial role of cGAS-STING in depleted cells which were no more able to up-regulate p16, p21 and SASP, and so to induce senescence. The main factors released by cells that has undergone to VIS, included in SASP definition, are mainly related to NF-kB targets. Indeed, infected cells are characterized by senescence markers such as β-galactosidase activity, up-regulation of IL-6 and IL-8 and ROS release.

This feature is typical of patients characterized by a VSV infection: senescent status reduces the infectivity of the cells and makes them less permissive to viral replication. The key player of this resistance is the senescence-associated secretory phenotype. Furthermore, SASP activates the immune system, especially natural-killer cells (NKs) and dendritic cells (DCs), to clear infected cells supporting the viral depletion. These features have been highlighted in during SARS-CoV-2 infection. Indeed, this infection is most common in elderly people yet characterized by a high percentage of senescent cells and a strong immune response associable to SASP release.

Finally, SASP composition has been demonstrated to induce a paracrine damage in the neighbouring non-infected cells.

In this context, SASP factors contribute to ‘cytokine storm’, tissue-destructive immune cell infiltration, endothelialitis, fibrosis and micro-thrombosis. SASP-driven spreading of cellular senescence due to COVID-19 was observed in different tissues, such as lung, kidney and brain, even when the infection was resolved, suggesting that SASP and the cytokine storm evocated are responsible for organ aging and long Covid disease. In addition, senescence markers such as $p16^{INK4a}$, $p21^{WAF1/Cip1}$, and histone H2AX were observed in mouse models of COVID-19 not only in tissue with active virus replication but also in virus-negative portions, suggesting that the inflammatory action of SASPs may induce premature organ aging. Overall, these results suggest innate immune pathways enforce both growth arrest to inhibit viral replication and prevent further spread of pathogens. Senescence may be an evolutionary mechanism for promoting antiviral defense. Therefore, research focusing on VIS and SASP in these contexts is urgently needed as it may open new therapeutic approach in order to counteract viral infection and the spread of aging profiles induced by viruses.

2. OBJECTIVE OF THE THESIS

The work of this thesis is to assess a complete the characterization of the senescent phenotype induced by Human Cytomegalovirus (HCMV) infection in human kidney cells. Specifically, we aim to evaluate the senescent profile of infected cells and investigate the response of adjacent non-infected cells to determine if paracrine senescence is a consequence of the infection. This involves analysing key markers of cellular senescence, such as alterations in gene expression, and the secretion of senescence-associated secretory phenotype (SASP) factors. Additionally, we will explore the molecular mechanisms by which infected cells communicate with neighbouring cells, potentially inducing a senescent state in the latter. By delineating these processes, we will explain how HCMV-induced senescence may contribute to kidney-specific pathogenesis.

3. MATERIALS AND METHODS

3.1 Cells and virus

Human foreskin fibroblast (HFFs, ATCC SCRC-1041) and ARPE-19 (ATCC CRL-2302) were grown in high-glucose Dulbecco'smodified Eagle's medium (DMEM, Sigma-Aldrich, Milan, Italy) supplemented with 10% fetal bovine serum (FBS, Sigma-Aldrich)) and 1% penicillin-streptomycin-gentamycin solution. hTERT-immortalized human renal proximal tubular epithelial cells (RTECs h-Tert, Evercyte GmbH, Wien, Austria) were cultured in ProxUp Supplement media (MHT 003-2, Evercyte GmbH).

HCMV TR strain was propagated one passage in HFFs and two passages in ARPE-19 cells. A standard plaque assay was performed on confluent HFFs to titrate the virus. 2.5×10^4 HFFs were seeded in 96-well plates in DMEM supplemented with 10% FBS. Serial dilution of HCMV TR strain, from 10^{-1} to $10^{-7,}$ were then added to HFFs in duplicate, and cells were centrifuged at 3000 rpm for 30 min, and then incubated for 2 h at 37 °C. HCMV TR solution were then discarded, and cells were layered with 0.8% methylcellulose. After 8 days, the methylcellulose layer was removed, and cells were stained with 0.1% crystal violet for 30 min on a shaker, then washed with water, and air-dried. The plaques were manually counted under a microscope.

For each experiment, 5 x 10^4 RPTECs and ARPE-19, and 7 x 10^4 HFFs were seeded in 6-well plates. RPTECs, HFFs and ARPE-19 cells were infected at an MOI 1, 0.5 and 3 respectively; and the infection was stopped after 24 hours by changing the media. Cells were then observed from 1 dpi to 8 dpi, considering the time of infection as day zero. The mock samples were the non-infected ones.

In case of infection with the IL-6R inhibitor, TCZ, monoclonal antibody against IL-6 receptor, (HY-P9917; MedChemExpress, MonmouthJunction,NJ,USA) was added to the cells at each media change, starting from the day of infection, at a concentration of 25 μg/ml.

3.2 Western Blot

RPTECs and ARPE-19 (5×10^4) and HFFs (70×104) were seeded in 6-well plates and infected with HCMV TR at an MOI of 1, 3 and 0.5, respectively, and then the cells collected each day post infection, from 1 to 6. Infected and non-infected cells were harvested from 1 dpi to 6 dpi and lysed with RIPA (Pierce) buffer supplemented with phosphatases inhibitor (Thermo Fisher Scientific) and protease inhibitor (Sigma-Aldrich) on ice. Total extracts were quantified using

Bradford reagent for the colorimetric reaction, reading the absorbance at 595 nm with a nanophotometer. Twenty μg of protein extracts were separated by electrophoresis on 7.5% and 12% SDS-polyacrylamide gels prepared with TGX™ FastCast™ Acrylamide Kit (Bio-Rad) and subsequently transferred to Trans-Blot® Turbo™ mini-size nitrocellulose (Bio-rad) using Trans-Blot® Turbo™ Transfer System (Bio-Rad). The membranes were blocked with 10% non-fat milk in Tris buffered saline-tween (TBST) and probed with specific primary antibodies overnight at 4°C. After washing with TBST, the specific HRP-conjugated secondary antibodies (anti-mouse or anti-rabbit) was incubated for 1 hour at room temperature. The binding was revealed using Clarity Max™ Western ECL Substrate (Thermo Fisher Scientific, Super Signal West Pico) and the bands were visualized in chemiluminescence using ChemiDoc™ MP Imaging System (Bio-Rad). Expression of β-actin was used as protein loading control.

3.3 Transcriptomic analysis

Total RNA from infected and parental RPTECs was isolated and subjected to high-throughput sequencing to analyze poly-A+ RNAs. Two biological replicates were analysed for each sample. RNA sequencing was performed with an Illumina NextSeq550 sequencer (Illumina, Inc.). In parallel, paired-end raw reads of parental and infected HFF and ARPE-19 cells were downloaded from GSE120891. These reads, together with those from parental and infected RPTECs, were analyzed using the fold lowing pipeline: The STAR program63 was used to align reads to the reference human hg38 genome. Ensemble v100 annotations were set as the reference for the RSEM computational pipeline64, which was employed to quantify gene expression levels. DEGs were calculated using DESeq265 with parameters of log2 fold change (log2FC) >2 and adjusted p-value (p.adj) < 0.05 to determine the statistical significance of DEG. All statistical and graphical computations were performed in the R environment (https://www.r-project.org/). Unsupervised hierarchical cluster ing of genes was visualized as a heatmap using the "heatmap" package in R, with expression values presented as log2. GSEA was employed to investigate the cellular response to HCMV infection. Gene Set Enriched Analysis was performed using the desktop application and significant GSEA terms were filtered using the following cut-offs: |NES|>1 and FDR.

3.4 EdU proliferation assay

RPTECs (1.5×10^4), ARPE-19 (2.5×10^4), and HFFs (3.5×10^4) were seeded in triplicate on coverslips in 24-well plates and infected with HCMV TR at an MOI of 1, 3 and 0.5, respectively. At 2 days post infection, EdU 50 μM was used to treat the cells for 20 hours. Cells

were then fixed with 4% paraformaldehyde, permeabilized with saponin 1% and then stained with the ClickTech EdU Cell Proliferation Kit 488 (baseclick GmbH, Neuried, Germany) and counterstained with DAPI according to the manufacturer's instructions. Images were acquired using a THUNDER Imager Live Cell & 3D system (Leica Microsystems) using the Navigation tool (63x magnification). For each sample, 16 fields were quantified in triplicates. The number of cells was counted through LAS X software (Leica Microsystems). The images were cropped using Microsoft PowerPoint (Microsoft 365, Version 2206, 2019).
Instead, in case of treatment with UVB-inactivated conditioned media, EdU 50 μM has been incubated for 20 hours starting from the second day post treatment. Then, the staining was performed as previously described.

3.5 SA-β-gal staining

Cell lines were seeded and infected as described for EdU proliferation assay At 3 dpi, the three cell lines were washed with PBS and fixed with fixative solution (2% paraformaldehyde plus 0,2% glutaraldehyde in PBS) for 4 minutes at room temperature. After two washing with PBS, 5 minutes each, cells were incubated overnight at 37°C, in absence of CO_2, with the staining solution containing the substrate X-gal. Then, after 3 washes with PBS, cells were stained with DAPI for at least 30 minutes before the acquisition. Raw images (2 × 2 montage) were acquired using a 4X objective with a Cytation 5 Cell Imaging Multi-Mode Reader (Agilent BioTek, Santa Clara, CA, USA), in both the fluorescent and bright-field channels to visualize nuclei and SA-β-gal positive cells, respectively, and then processed and stitched using the default setting of the proprietary software.

3.6 RNA extraction and library construction

For transcriptome analysis, mRNA was extracted using the miRNeasy Tissue/Cells Advanced Kit (Qiagen, Hilden, Germany). Samples quality was confirmed with Agilent 4200 TapeStation system and HS D1000 RNA kit (Agilent, Santa Clara, CA, USA), with all samples showing an RNA Integrity Number (RIN) > 8, indicating good quality of the extracted material. Library preparation was performed with an Illumina TruSeq Stranded mRNA kit (Illumina, Inc., San Diego, CA, USA) using 500 ng of total RNA per sample. mRNA sequencing was then performed on a NextSeq 550 platform (Illumina, Inc.) through NextSeq 500/550 High Output Kit v2.5 (150 Cycles - 2 × 75 read length, paired-end) (Illumina, Inc.).

3.7 Quantitative real-time PCR

Quantitative real-time PCR (qRT-PCR) was performed with a CFX96 Real-Time PCR Detection System (Bio-Rad Laboratories, Hercules, CA, USA), as previously described68. Total RNA was extracted using TRI Reagent (Sigma-Aldrich), and 1 μg was retrotranscribed using an iScript cDNA Synthesis Kit (Bio-Rad). Reverse-transcribed cDNAs were amplified in duplicate using SsoAdvanced Universal SYBR Green Supermix (Bio-Rad Laboratories). The 18 S gene was used as housekeeping gene for normalization of cDNA levels. The relative normalized expression after stimulation was calculated as fold change over control using the formula = 2 -Δ(ΔCT) where ΔCT = CTtarget—CT18S and Δ(ΔCT) = ΔCTstimulated - ΔCTcontrol. The primer sequences used in qRT-PCR experiments were as follows: LaminB1 FW 5′-AAG CAT GAA ACG CGC TTGG-3′, LaminB1 REV: 5′-AGT TTG GCA TGG TAA GTC TGC-3′; Ki67 FW 5′-TCC TTT GGT GGG CAC CTA AGA CCT G-3′, Ki67 REV 5′-TGA TGG TTG AGG TCG TTC CTT GAT G-3′; 18S FW 5′-TCC CCA GCC CTT TTG TTG A, 18S REV 5′-TTA GAA CCA AAT GTG GCC GTG-3′.

3.8 Multiplex immunoassay of cytokines/chemokines

Supernatants collected from infected or mock-infected RPTECs were screened for the presence of 27 human cytokines and chemokines using the Bio-Plex Pro^{TM} Human Cytokine Grp I Panel 27-Plex kit (Bio-Rad Laboratories). The analysis was performed with Bio-Plex 200 System (Bio-Rad Laboratories) according to the manufacturer's instructions.

3.9 ELISA

Secreted cytokines, specifically LCN2/NGAL, IL-6 and IL-8, were analysed in cultures supernatants after infection or treatment using the human LCN2/NGAL ELISA kit (Hycult Biotech, Uden, NL), human IL-6 DuoSet ELISA and human IL-8 DuoSet ELISA (both from R&D Systems) according to the manufacturer's instructions. Absorbance was measured using a Spark multimode microplate reader (Tecan, Männedorf, Switzerland).

3.10 Immunofluorescence microscopy

RPTECs (1.5×10^4), ARPE-19 (2.5×10^4), and HFFs (3.5×10^4) were seeded in triplicate on coverslips in 24-well plates and infected with HCMV TR at an MOI of 1, 3 and 0.5, respectively. After 2, 3, 4 and 6 day post infection, cells were fixed for 15 minutes at room temperature with 4% paraformaldehyde and permeabilized with 0,2% Triton-X100 on ice for

20 minutes at 4°C. To saturate the aspecific antigenic determinants samples were incubate for 15 minutes at room temperature with the blocking solution composed of PBS + 1% Bovine Serum Albumin (BSA) + 1% Normal Goat Serum (NGS) + 0.05% Tween-20. Then, cells were incubated with the appropriate dilution of primary antibody in a humidified chamber at room temperature for 1 hour. This step was followed by the incubation with secondary labelled antibody, goat anti-mouse IgG Alexa Fluor 488 (A11001, Thermo Fisher Scientific), and goat IgG anti Rabbit IGA-Alexa Fluor (A-11036, Thermo Fisher Scientific), supplemented with DAPI (4′,6′-diamodino-2phenylindole) (D1306, Thermo Fischer Scientific, Waltham, MA, USA) to counter-stain the nuclei for 1 hour. The coverslips were mounted with SlowFade Gold antifade reagent mounting media (Thermo Fischer Scientific), and cells were visualized using a Leica Thunder Imager 3D System (Leica Microsystems, Wetzlar, Germany). The percentage of infected cells expressing IEA, UL44, and pp28 and the percentage of positive cells displaying NF-κB, $p16^{INK4a}$ and γH2AX for each cell line were normalized to the total number of DAPI-positive cells. Image analysis was carried out using the LAS X software (Leica Microsystems), and values were expressed as mean ± SD (error bars).

3.11 Antibodies

The following primary and secondary antibodies were used: monoclonal anti-HCMV IEA (P1215, Virusys Corporation, Taneytown, MD, USA) or in house-produced rabbit polyclonal anti-IEA62, monoclonal anti-HCMV pp28 (P1207, Virusys Corporation), monoclonal anti-HCMV UL44 (P1202, Virusys Corporation), monoclonal NF-κB (L8F6 6956, Cell Signaling Technology, Danvers, MA, USA), rabbit monoclonal $p16^{INK4a}$ (E6N8P) (18769 S, Cell Signaling Technology), γH2AX (JBW301, Sigma-Aldrich), goat anti-mouse IgG-Alexa Fluor 488 (A11001, Thermo Fisher Scientific), and goat IgG anti-Rabbit IGA-Alexa Fluor (A-11036, Thermo Fisher Scientific).

3.12 Plaque assay

To determine the infectivity of the supernatants, a standard plaque assay was carried out on HFFs. Briefly, 2.5×10^4 HFFs were seeded in 96-well plates in DMEM supplemented with 10% FBS. Supernatants from HCMV-infected RPTECs, ARPE-19 or HFFs—diluted from 10−1 to10−7—were then added to HFFs in duplicate, centrifuged at 3000 rpm for 30 min, and incubated for 2 h at 37 °C. Supernatants were then discarded, and cells were layered with 0.8% methylcellulose. After 8 days, the methylcellulose layer was removed, and the cells were

stained with 0.1% crystal violet, incubated at RT for 30 min on a shaker, washed with water, and dried. The plaques were manually counted under a microscope.

3.13 Conditioned media treatment

In case of treatment with conditioned media, the supernatants were collected after 3 days of infection, centrifuged at 10,000g for 5 min, treated using double pulse of UVB light (1.2 J/cm2), and used to treat freshly seeded cells for additional 3 days. Next, proliferation was evaluated by the EdU assay in presence or absence of the IL-6R inhibitor TCZ at a concentration of 25 μg/ml.

In case of starvation media treatment, the supernatants were collected after 5 days of culture, centrifuged at 10,000g for 5 min, and used to treat freshly seeded cells for additional 3 days. In this condition, proliferation was evaluated by the EdU assay in presence or absence of the IL-6R inhibitor TCZ at a concentration of 25 μ g/ml.

4. RESULTS

4.1 HCMV infection characterization

To investigate the impact of HCMV infection on renal proximal tubular epithelial cells, RPTECs—of note, these cells are hTERT-immortalized cells retaining normal morphological and functional properties with no genomic instability —were infected with the HCMV TR strain . Human foreskin fibroblasts (HFFs) cells were included as control of infection as the principal cellular models of HCMV infection; instead, adult retinal pigment epithelial cell line (ARPE-19) was chosen as epithelial positive control for the infection.

To understand and study the viral life cycle in the three cell models, we performed a western blotting to investigate the differential expression of the three main marker (protein) representative of the different phase of the replication cycle: immediate-early (IE), early (E), and late (L). Specifically, we observed IE1 and IE2 between 1 and 2 dpi in all three cell lines and remained at high levels until 6 dpi. Then, we detect the early protein UL44 from the 2 or 3 dpi, and the late protein pp28 started its expression at 3 dpi in RPTECs and ARPE-19 cells but at 4 dpi in HFFs (Figure 6A).

We also performed immunofluorescence technique to study the amount of infected cells. As shown in Figure 6B, IEA is expressed in 72-80% of the cells, in all the three line, since 2 dpi; UL44 expression was found in 70% of HFFs and ARPE-19 cells but only in 33% of RPTECs at 4dpi. This result is consistent with the previous one obtained by western blotting. A similar trend was observed with the late protein pp28, which was expressed in 80% in HFFs and ARPE-19 cells, and in 35% in RPTECs at 6 dpi.

To demonstrate the productivity of HCMV infection in RPTECs, we measured virus yield in the supernatants from infected cells at 4 and 6 dpi. The results in Figure 6C shown that HFFs were characterized by the highest viral production (~3×10^3 and 2×10^5 PFU/mL, at 4 and 6 dpi respectively). This value decreased in ARPE-19 cells and RPTECs (~5×10^2 and ~1.7×10^4 PFU/mL and ~1×10^3 and ~6×10^3 PFU/mL, respectively).

Overall, these results confirm that these three cell lines support the HCMV productive cycle with the spread of new virions in the supernatants. However, RPTECs were less efficient in terms of viral protein expression, especially the early and late ones, and in terms of viral load results compared to the other two models.

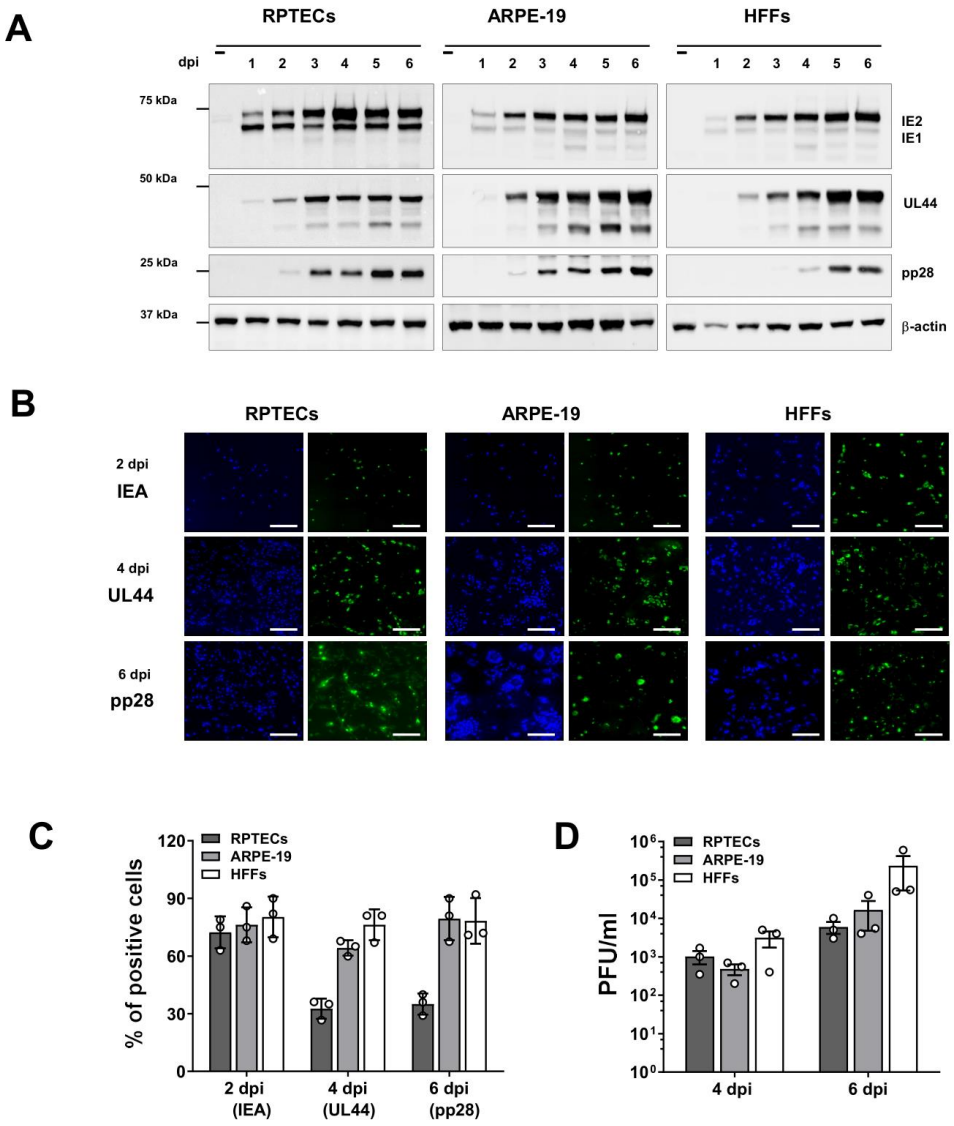

Figure 6. Characterization of HCMV infection on RPTECs, ARPE-19 cells and HFFs. **A.** *Western Blot analysis shows the viral kinetic expression of RPTECs, ARPE-19 and HFFs infected cells. The expression pattern is similar through the three cell lines: IEA starts at 1 dpi and pick at 3 dpi; UL44 is expressed at 2 dpi ant pick at 4 dpi and pp28 is detected at 3 or 4 dpi and pick at 6 dpi.* **B.** *Immunofluorescence analysis for viral proteins detection revealed IEA positive staining (green) for 75% in all the three cell lines, UL44 positive staining (green) for 33% of RPTEC compared to 70% of ARPE-19 and HFFs; and pp28 positive staining (green) for 35% of RPTEC compared to 80% in ARPE-19 and HFFs. DAPI was used for nuclei staining (blue). The percentages of cells expressing viral genes represent the mean of three replicated experiments. Values were expressed as means ± SD (error bars).* ***C.*** *The production of viral particles in RPTECs, ARPE-19, and HFFs infected with HCMV TR was*

measured by plaque assay on HFFs. At 4 and 6 dpi, viral plaques were microscopically counted and expressed as PFU/mL. Values are expressed as means ± SD (error bars) of three independent experiments.

4.1 Transcriptomic analysis and associated secretory phenotype: deeper inside the HCMV infection

In order to investigate the impact of HCMV in renal infection, we characterized the transcriptomic profile of kidney cells in comparison with the other cell model of infection. RPTECs were infected as previously described and at 48h post infection, we performed a poly-A^+ RNA sequencing of the HCMV vs mock-infected- cells. As regard fibroblasts and epithelial cells as positive control, we based on public database of transcriptomic[35]. First, the differentially expressed gene (DEG) of the three cell lines were compared to the available data in the GEO database. Functional annotation of DEGs between HCMV- and mock-infected cells for each cell line showed significant enrichment in several biological processes, as shown in Figure 7B. HCMV-infected RPTECs and HFFs but not in ARPE-19 cells, showed a common enriched DEGs profile of the following biological processes: "response to virus", "response to type I interferon", "regulation of response to biotic stimulus", "regulation of defense response" and "positive regulation of cytokine production". However, HCMV-infected ARPE-19 cells showed almost equal enrichment of processes such as "response to growth factor", "regulation of growth", "regulation of epithelial cell proliferation", "epithelial cell differentiation", and "regulation of morphogenesis of an epithelium". Note of worthy, the gene ontology (GO) term "inflammatory response" was identified specifically in HCMV-infected RPTECs, but not in the other two cell lines. The analysis of DEGs associated with the "inflammatory response" revealed high expression levels of several paradigmatic inflammatory cytokines, such as IL-6, IL-1β, CXCL8 (IL-8), CCL5 (RANTES) and CXCL10 (IP-10), in infected RPTECs, as show in Figure 7B. Interestingly, there is no significant variation of these DEGs in the ARPE-19 cells and HFFs post infection. Furthermore, we performed a gene set enrichment analysis (GSEA) based on the hallmark terms of HCMV-infected vs mock RPTECs, ARPE-19 cells and HFFs as shown in Figure 7C. This analysis highlighted the enrichment of the "hallmark allograft rejection" present only in the gene set of RPTECs and the enrichment of the "hallmark IL6-JAK-STAT3 signalling", two hallmarks of renal injury and strictly connected with organ damage [36]. As many of the cytokines we found to be upregulated in HCMV infected RPTECs had previously been linked to SASP, we took advantages of the Sen Mayo signature, able to

predicts senescence-associated pathways across various tissues. The analysis shown in Figure 7D, emphasized an enrichment of senescence genes in the RPTECs and in the HFFs (FDR q-value = 0.000 and = 0.002, respectively), but not in the ARPE-19 cells (FDR q-value = 0.70). Overall, these results shown i) a unique inflammatory profile present in the RPTECs that resemble in a rejection signature and ii) a connection between the HCMV-infection and senescence induction in RPTECs and HFFs that is not evident in ARPE-19.

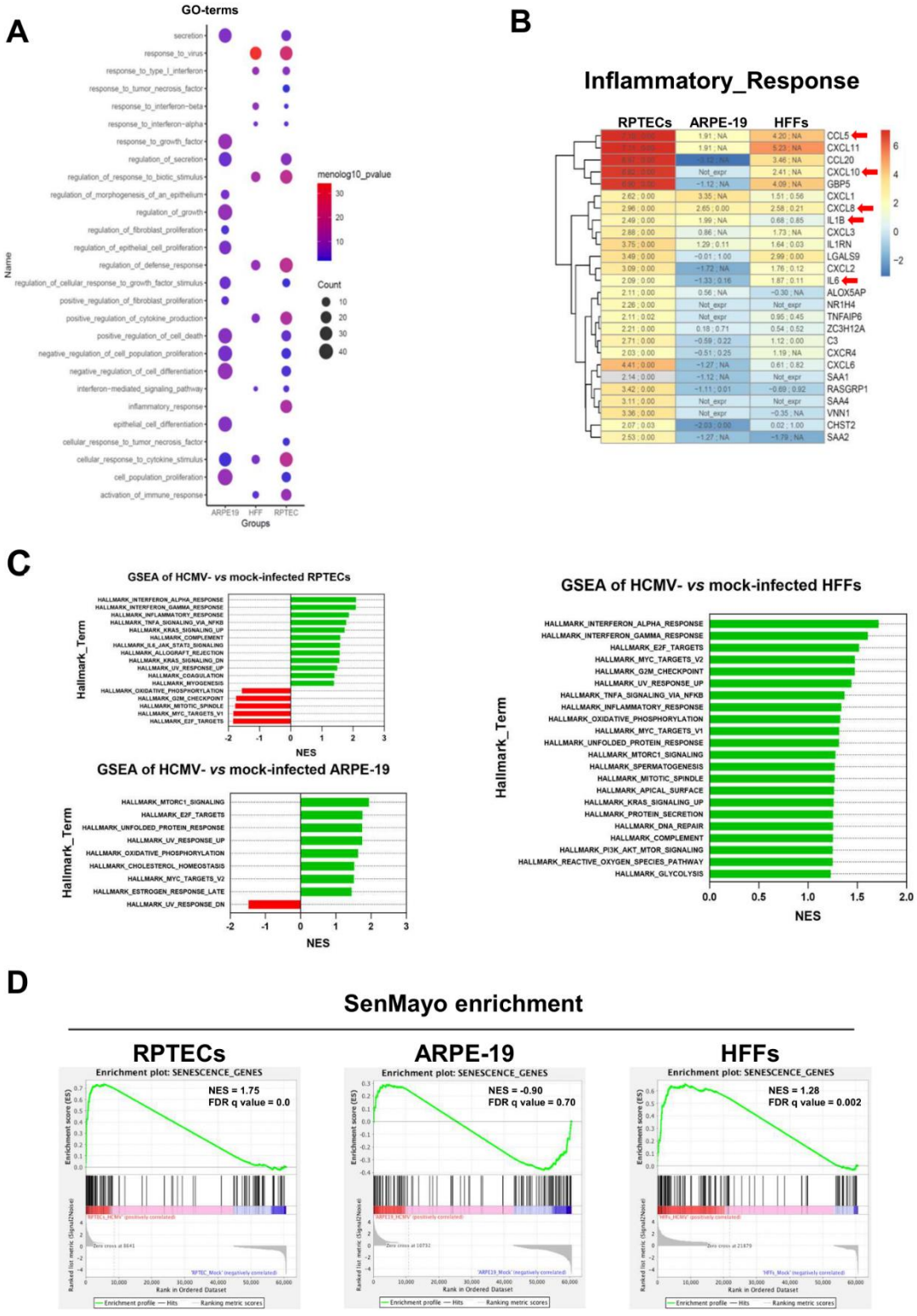

Figure 7. Bioinformatics analysis to identify the typical signature of response upon HCMV infection. A. *Representation of Gene ontology (GO) term in RPTECs, HFFs and ARPE-19*

cells. The dot dimension represents the number of genes enriched in that cell lines; the colour vary basing the Log-10 enrichment. ***B.*** *Heatmap representative of the differentially expressed genes (DEG) of inflammatory response in RPTECs, ARPE-19 cells and HFFs. The study has been based to compare HCMV- versus mock-infected condition basing on the GO term response.* ***C.*** *Gene set enrichment analysis (GSEA) was performed on RPTECs, ARPE-19 and HFFs, HCMV- versus mock-infected. Green bars indicate a positive enrichment; red bars indicate a downregulation in virus-positive cells.* ***D.*** *GSEA of the comparison between HCMV-infected and mock-infected cells, showing the enrichment of senescence genes associated with the SenMayo signature in RPTECs and HFFs. The enrichment score curve is depicted in green, with genes on the far left (red) correlating with HCMV-infected cells, and genes on the far right (blue) correlating with mock-infected cells. The vertical black lines indicate the position of each gene in the gene set analyzed. NES and FDR are shown.*

To better characterise the inflammatory response evoked by HCMV upon the infection in RPTECs, we performed a Bio-Plex analysis to compare the different secretion level of cytokines in HCMV-infected vs mock RPTECs supernatants from the first to the fifth days post infection. The results reported in Figure 8A showed an accumulation of the inflammatory cytokines, such as GM-CSF, MIP-1α, IP-10, RANTES, TNF-α, IL-6, IL-8, IL-9 in infected supernatants in comparison with mock counterparts. In particular, the up-regulation of IP-10 in infected cells is a confirmation of the previous data because its involvement in the kidney graft rejection[37], since it is a chemo attractor correlated with acute tubular injury and acute rejection transplantation. GM-CSF, MIP-1α, IP-10 increase gradually in the course of infection, reaching maximum secretion on the fifth day after infection, but this increase was not observed in non-infected cells. Instead, the up regulation of RANTES in infected cells detected at 5 dpi, is significative because it is a senescence marker[38]. Lastly, IL-6, IL-8 and IL-9 are up-regulated from the first day after infection, while TNF-α picked at 4 days post infection with no further induction at later time points post infection.

Finally, in order to connect the inflammation observed upon infection with tubular injury and damage, we investigated the expression and the release in the supernatants of Lipocalin 2 (LCN2), a well-known renal-injury marker[39]. The increased mRNA levels and the presence of proteins in the supernatants of HCMV-infected cells but not in the mock counterparts, confirm the induction of damage in the sample (Figure 8B).

Overall, the results so far obtained underlined a robust and unique pro-inflammatory response in kidney cells, together with signs of tubular damage upon HCMV infection.

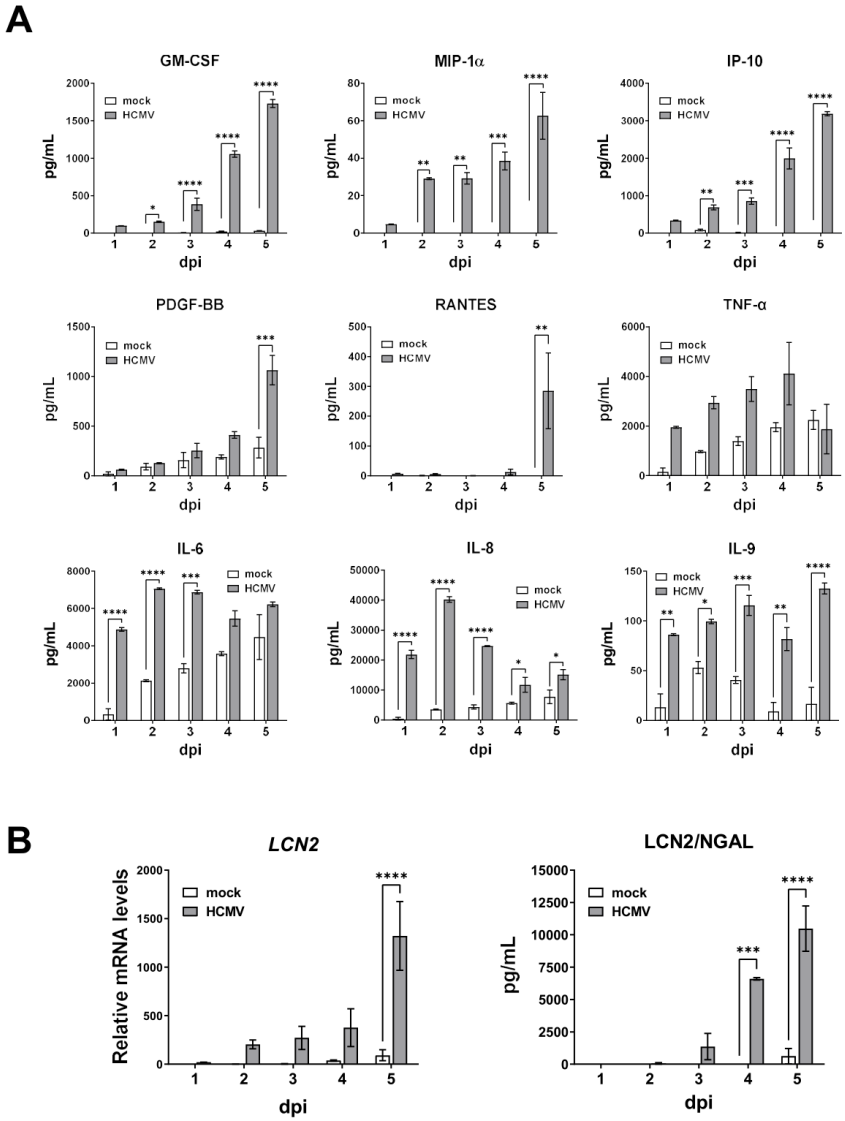

Figure 8. Detection to evaluation of the inflammatory and damage response in kidney cells during HCMV infection. A. *Multiplex immunoassay analysis of secreted cytokines and chemokines in the supernatants from HCMV-infected RPTECs at different time points of infection (MOI1). The assay detected 27 secreted molecules, these 9 reported above are the most present in the supernatant: granulocyte-macrophage colony stimulating factor (GM-CSF), macrophage inflammatory protein 1-alpha (MIP-1 α/CCL3), interferon-inducible protein 10 (IP-10/CXCL10), platelet-derived growth factor-BB (PDGF-BB), regulated upon activation, normal T-cell expressed and secreted (RANTES), tumor necrosis factor-alpha (TNF-α), interleukin-6 (IL-6), interleukin-8 (IL-8), interleukin-9 (IL-9).* ***B.*** *qPCR analysis of RNA expression for lipocalin 2 or neutrophil gelatinase-associated lipocalin (LCN2) at different time points of infection, HCMV- mock-infected RPTECs. The graph on the*

right side of the panel represents ELISA measurement of the secreted protein (LCN2/NGAL, right panel) at the same time points.

4.3 Cellular senescence marker upon infection

Based on the results obtained from the transcriptomics analysis and the identification of SASPs in the HCMV-secretome, the next step included the analysis of senescence markers in order to investigate possible damage following infection.

First, we measured the senescence-associated β-galactosidase (SA-β-gal) activity at neutral pH to evaluate the senescent profile of the cells. As the Figure 9B shown, HCMV-infected RPTECs and HFFs display an increased SA-β-gal activity that is linkable with a senescent phenotype. Specifically we infected RPETCs at MOI 1, HFFs at MOI 0,5 and ARPE-19 cells at MOI 3 for 24 hours before stopping the absorption; these different conditions of infection allow to obtain a comparable infection between the different cell lines. In particular, we measured 88% of HCMV-infected SA-β-gal positive RPTECs versus 44% in the mock counterparts; instead, in HFFs we detected 45% beta-gal positive-infected cells versus 8% positivity in mock ones. Both these variations were statistically significant. However, ARPE-19 cells are not characterized by any variation of the SA-β-gal activity between infected and non-infected cell culture. Consistently, the cells capability of EdU incorporation demonstrated a decrease of replication rate. In particular, RPTECs and HFFs are characterized by a decreased EdU incorporation in HCMV-infected cells and by a decreased number of cells per field. In particular, the data shown 33% of EdU positive RPTECs 3 days post infection versus 77% of EdU positivity in mock sample (Figure 9 D). As for the HFF cells, the results of the EdU incorporation showed a less significant variation between the infected samples and the non-infected counterpart.

On the other hand, ARPE-19 cells have not a significative EdU incorporation reduction between HCMV-infected and mock cells. Moreover, both in RPTECs and HFFs we observed a significant reduction in the number of cells per well ($P < 0.05$ in both cell lines), while we did not detect any significant changes in the number of cells per well between infected- vs mock ARPE-19 ($P > 0.05$).

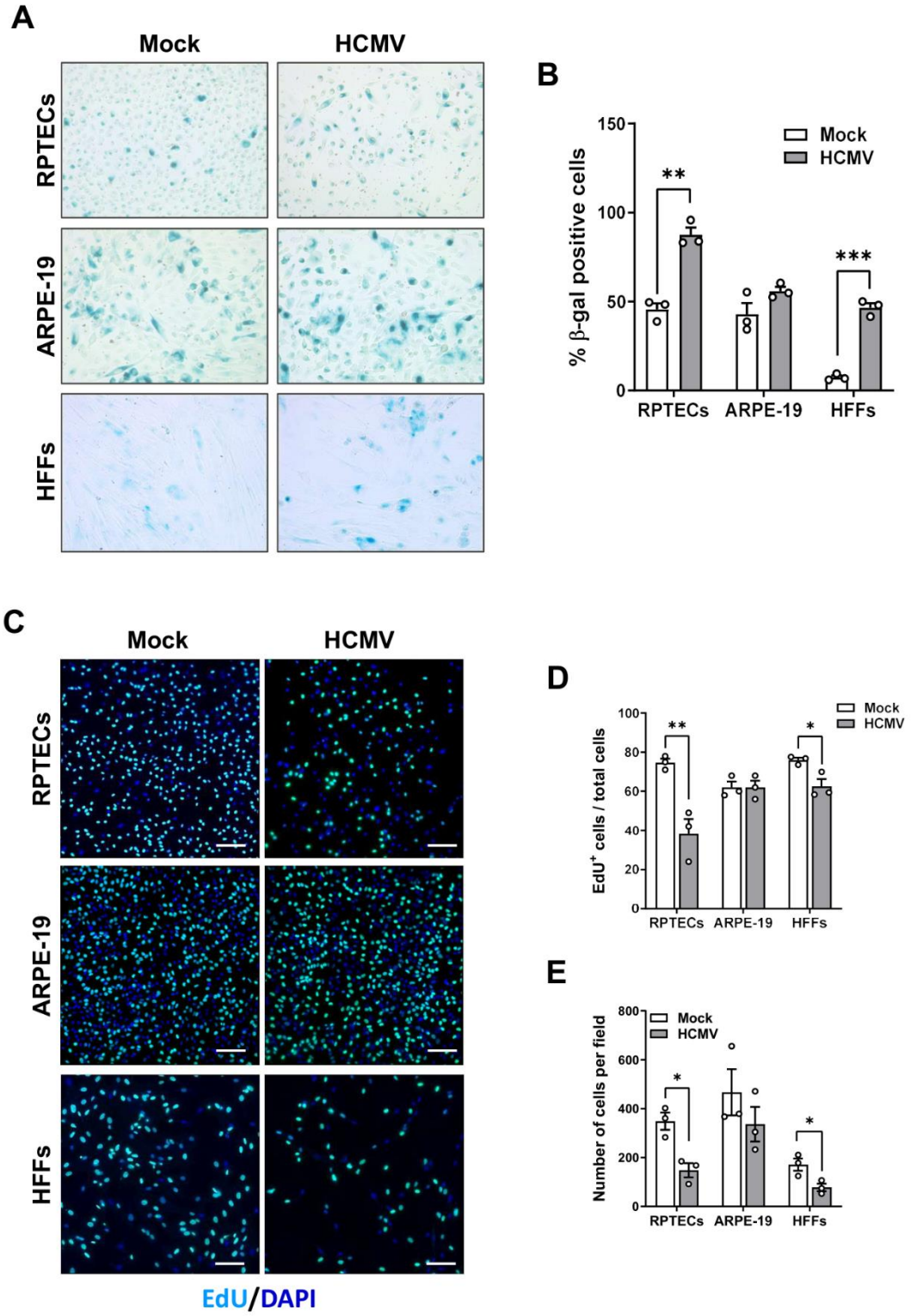

Figure 9. HCMV infection evocates senescence phenotype in RPTECs and HFF but not in ARPE-19. A. *Representative images of SA-β-gal staining of HCMV- or mock-infected RPTECs, ARPE-19 cells and HFFs. The analysis has been performed 3 days post infection, respectively at MOI 1, 3 and 0,5. The SA-β-gal staining correspond to the blue regions within the cells.* ***B.*** *Percentage of SA-β-gal positive cells among the three cell lines. There is a significative difference between HCMV-*

and mock-infected in RPTECs and HFFs. ***C****. 3 days post infection, RPTECs, ARPE-19 cells and HFFs, respectively at MOI 1, 3, 0,5, were incubated with EdU for 20 h and stained as described in the Material and Methods section. DAPI was used to counterstain the nuclei.* ***D-E.*** *These graphs show respectively the percentage of EdU+ positive cells and the total number of cells among the three cell lines*.

Then, we evaluated the mRNA level of *MKi67*, a proliferation marker, and *LAMINB1*, a marker of chromatin changes associated to senescence to confirm if senescence is occurring upon infection. Interestingly, we noticed a significative mRNA *MKi67* and *LAMINB1* level reduction only in HCMV-infected RPTECs but not in HFFs or ARPE-19 cells.

Finally, we evaluated the secretion of IL-6 and IL-8 upon HCMV infection due to their involvement in the senescence induction. Specifically, we evaluated these two cytokines into the HCMV-infected and mock supernatants through an ELISA. The goal of the experiment was to detect a release fluctuation consistent with an ongoing senescence profile in infected sample when compared to the mock counterpart. The data shown a higher release of IL-6 and IL-8 in HCMV-infected RPTECs and HFFs than mock counterparts (IL-6: ∼6-fold and ∼8-fold in RPTECs and HFFs, respectively; IL-8: ∼4-fold and ∼8-fold in RPTECs and HFFs, respectively) (Figure 10B). Instead, we did not reveal any significative variation into ARPE-19 cells supernatants. To further confirm the involvement of IL-6 in the infection, we performed a UVB-HCMV infection; we infected the three cell lines with an inactivated virus unable to replicate. In all the cell lines there were no significant variation of the IL-6 secretion between infected and mock samples as shown in Figure 10C. These results demonstrated the necessity of a replicative virus to induce the secretion of IL-6. Similarly, we did not detect any EdU incorporation variation between UVB-HCMV- and mock-infected cells. These results were confirmed in all the three cell lines.

The results shown in Figure 10 highlighted a senescence phenotype in RPTECs and HFFs that was not characteristic of ARPE-19 cells. In particular, this signature is more relevant in RPTECS. The data show the presence of senescence markers that are associable with the release of SASP-conducible cytokines, in particular IL-6 and IL-8.

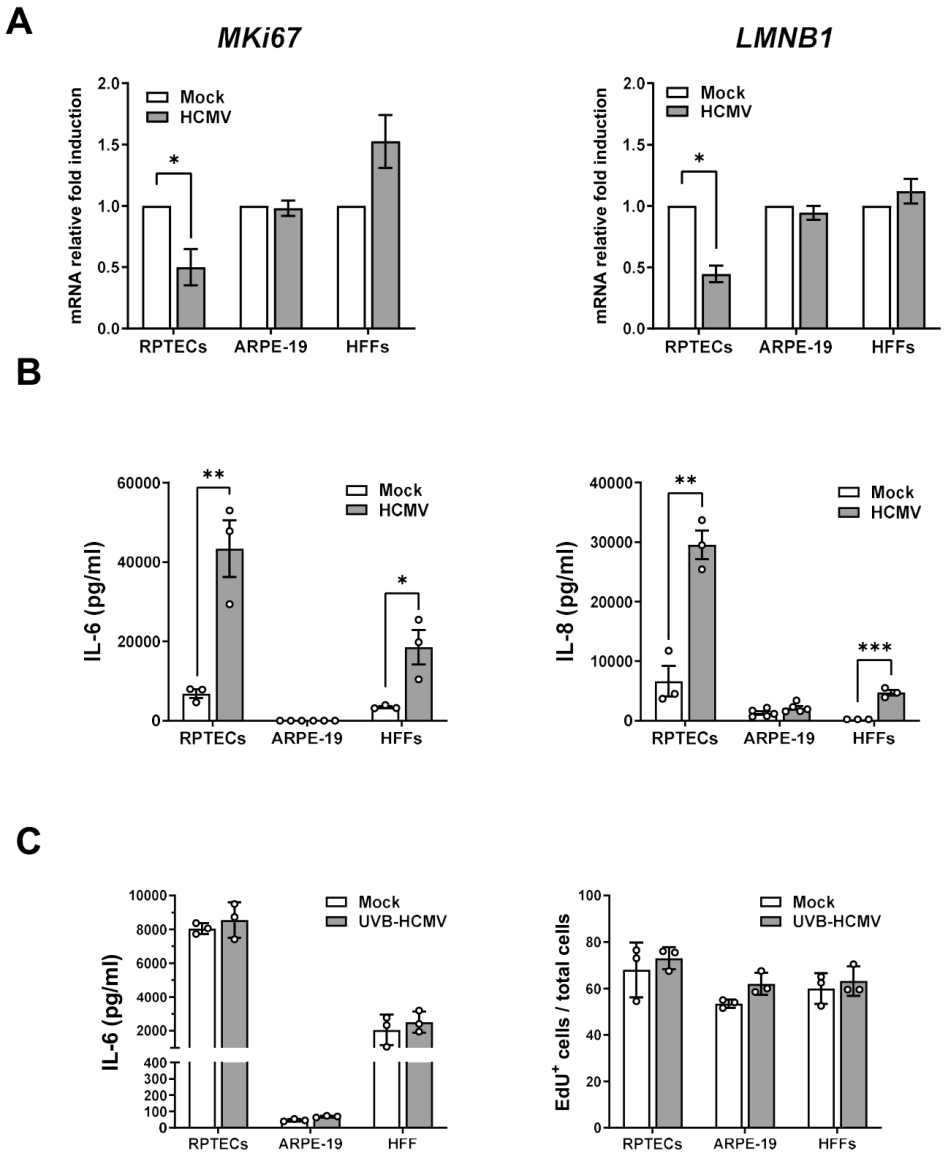

Figure 10. Signature of inflammatory and senescence phenotype in HCMV-infected cells.

A. *Quantitative PCR (qPCR) analysis was performed to measure mRNA expression levels of MKi67 and LAMINB1 from total RNA extracts collected at 3 days post-infection (dpi). Values were normalized to 18 S gene expression and presented as fold induction compared to mock-treated cells..* ***B.*** *IL-6 and IL-8 were detected in the supernatants- HCMV- vs. mock-infected cells by ELISA. The analysis has been performed on RPTECs, ARPE-19 cells and HFFs at 3 days post infection.* ***C.*** *The analysis of released IL-6 was used as marker to study the impact of UVB-HCMV infection. This evaluation was also performed exploiting EdU proliferation assay 3 days post infection.*

4.4 Induction of paracrine senescence upon HCMV infection of RPTECs

To better elucidate the senescence phenotype evocated by HCMV in the infected cells, we performed a co-staining for inflammatory and damaged markers linked to senescence, with viral protein. In particular, we performed immunofluorescence analysis on HCMV-infected and mock cells in order to detect NF-kB, γH2AX and $p16^{INK4a}$ simultaneously with IEA.

HCMV-infected RPTECs and HFFs showed the nuclear translocation of NF-kb which coincided with the expression of viral IEA (Figure 11A and C). Interestingly, a high percentage of NF-kB positive RPTECs were not positive for IEA ($P < 0.01$; Figure 11D), suggesting a spread of inflammatory activation into bystander cells. ARPE-19 cells, instead, were not at all characterized by a strong inflammatory response since the NF-kB levels were lower than RPTECs and HFFs overall.

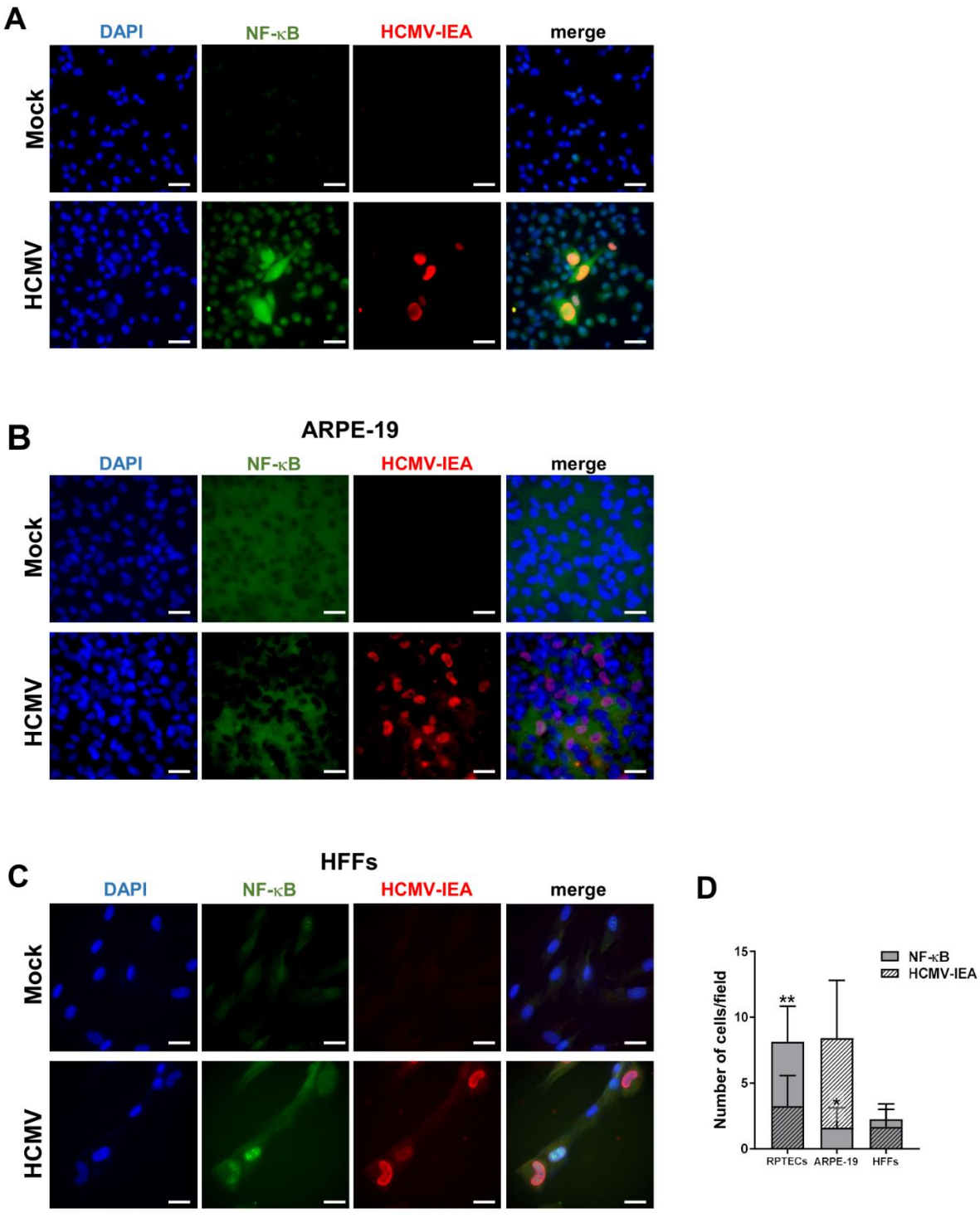

Figure 11. HCMV-infection induce NF-kB translocation in uninfected RPTECs but not in ARPE-19 and HFFs. A. *Microscopy imaging analysis of NF-kB translocation in HCMV- mock-*

*infected RPTECs, ARPE-19 (**B**) and HFFs **(C)**. Representative immunofluorescence co-staining of NF-kB in green with Immediate Early antigen (IEA) in red to detect the uninfected cells characterized by the translocation of the transcription. The cells were marked with DAPI staining in blue. The analysis was performed at MOI 1, 3, and 0,5, respectively, at 3 dpi. **D**. Histograms representation of the number of NF-κB and IEA-positive cells per field in HCMV-infected cells*.

The second marker investigated was the phosphorylated form of γH2AX because of the bound between senescence and DNA damage and, furthermore, due to the chromosomal instability consequence HCMV infection. RPTECs ere the only cell line showing a significative expression of γH2AXin non-infected cells ($P < 0.005$). In fact, neither HFFs or ARPE-19 cells showed this paracrine pattern as presented in the graph in Figure 12D. However, ARPE-19 cells are characterized by the higher expression of γH2AX in infected cells. Finally, we evaluated p16 expression due to its involvement cell cycle regulation. As the previous data shown, only RPTECs expressed significative level of p16 in a paracrine manner ($P<0.005$). Conversely, $p16^{INK4a}$ staining was solely restricted to infected HFFs, whereas ARPE-19 cells showed nuclear $p16^{INK4a}$ reactivity in less than 50% of the IEA-positive cells (Figure 13B). All these results confirmed the presence of a further paracrine-senescence pattern induced by HCMV-infection only in RPTECs but not in the HFFs or ARPE-19 cells.

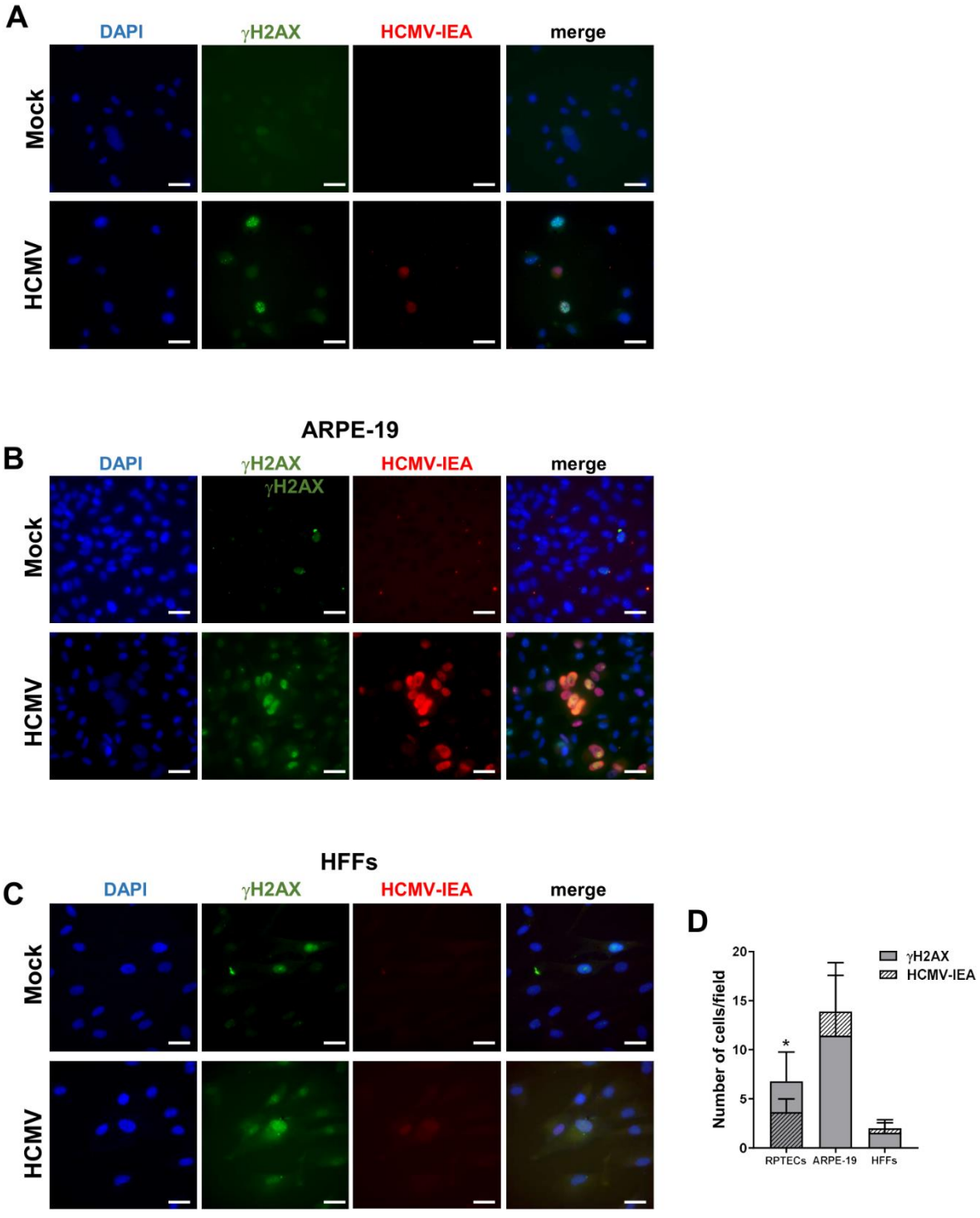

Figure 12. HCMV-infection induce the phosphorylated form of the histone γH2AX in uninfected RPTECs but not in ARPE-19 cells and HFFs. A. *Microscopy imaging analysis of phosphorylation form of* γH2AX *in HCMV- versus mock-infected RPTECs, ARPE-19 (**B**) and HFFs (**C**). Representative immunofluorescence co-staining of γH2AX in green with Immediate Early antigen*

(IEA) in red to detect the uninfected characterized by the phosphorylation form of the histone. The cells were marked with DAPI staining in blue. The analysis was performed at respectively MOI at 3 dpi. ***D****. Histograms representation of the number of* $\gamma H2AX$ *and IEA-positive cells per field in HCMV-infected cells*.

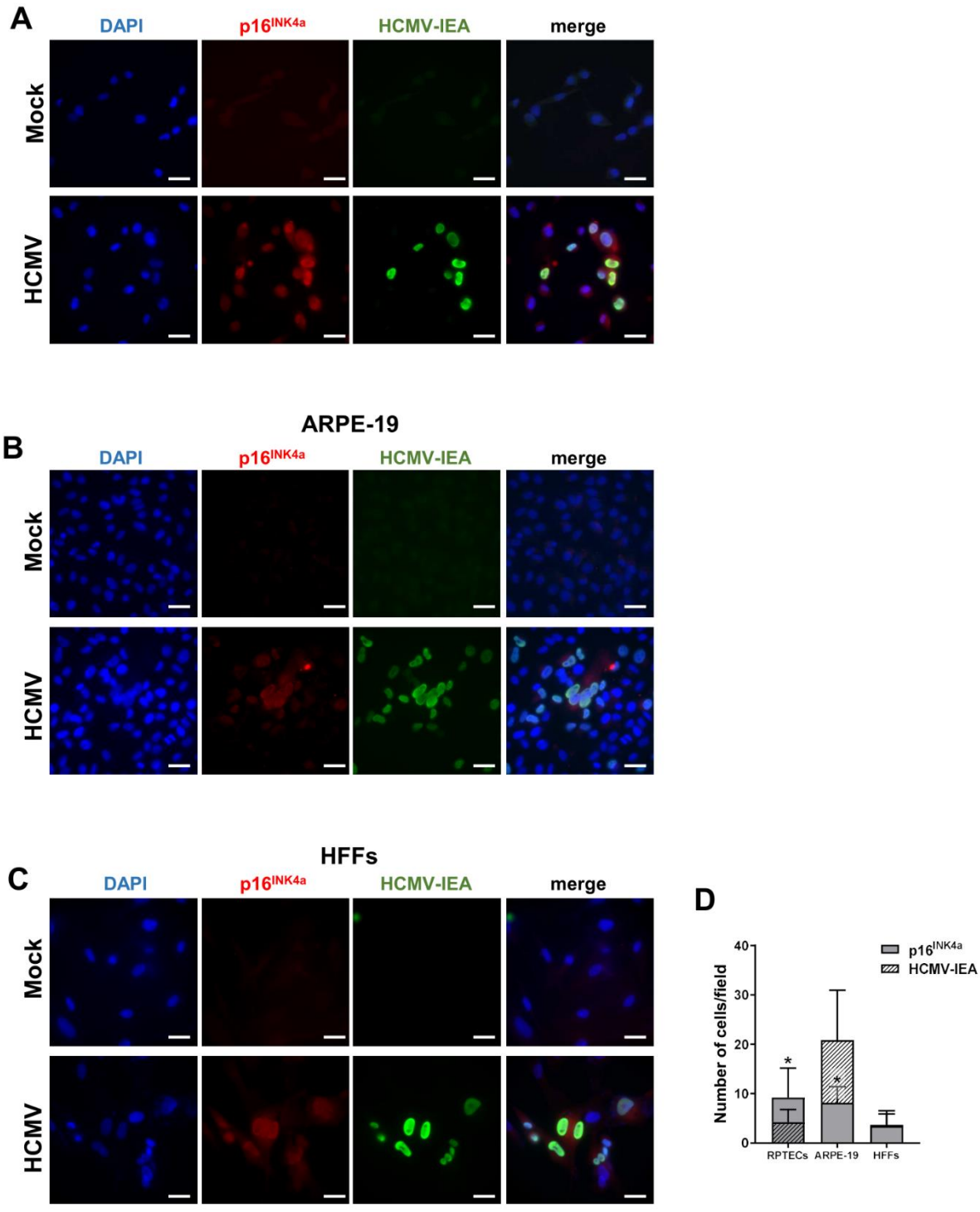

Figure 13. HCMV-infection induces p16 expression in uninfected RPTECs but not in ARPE-19 and HFFs. A. *Microscopy imaging analysis of p16 expression in HCMV- mock-infected RPTECs, ARPE-19 (**B**) and HFFs (**C**). Representative immunofluorescence co-staining of p16 in red with Immediate Early antigen (IEA) in green to detect the uninfected characterized by the expression of p16.*

The cells are marked with DAPI staining in blue. The analysis has been performed at MOI 1, 3 and 0,5, respectively, at 3 dpi. ***D****. Histograms representation of the number of p16 and IEA-positive cells per field in HCMV-infected cells*.

Based on the transcriptomic analysis result and specifically the enrichment of the "hallmark of IL-6/JAK-STAT3 signalling" in HCMV *vs* Mock RPTECs, we evaluated the paracrine senescence due to IL-6, especially due to the fact that this pathway has been implicated in paracrine senescence induction[36]. Therefore, we decided to perform an infection in presence of tocilizumab (TCZ), a monoclonal antibody that inhibits IL-6 receptor without interfering with the release of IL-6 itself. Specifically, we investigate the involvement of IL-6 in the paracrine senescence induction. We evaluated γH2AX and NF-kB expression in RPTECs at 3 days post infection, in presence or absence of TCZ. In case of treatment, both of the damage markers were significantly reduced in non-infected bystander cells which was limited to about 50% of IEA-positive cells ($P<0.05$ Figure 14). This results demonstrated a reduction of the spread of DNA damage signal and a reduction of nuclear translocation in neighbouring cells. We could assume that this change of pattern is due to the inability of IL-6 to bind and activate its receptor.

The data showed the translocation of inflammatory and damage markers in uninfected RPTECs but not in the other two cell lines. Furthermore, the central role of IL-6 in these data demonstrated the presence of a paracrine senescence-like phenotype induced by the infection itself in RPTECs.

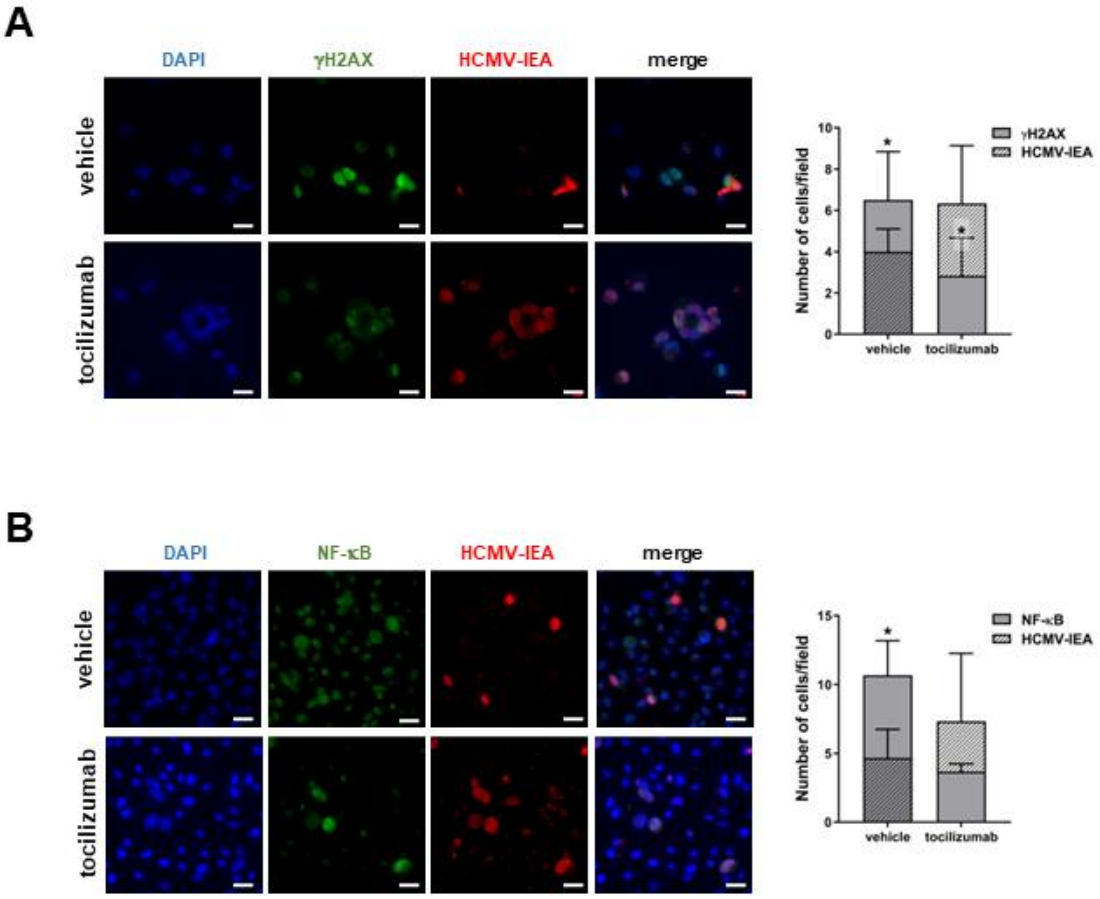

Figure 14. Evaluation of the paracrine damage and inflammation upon infection of RPTECs in presence of TCZ. A-B *Representative immunofluorescence co-staining of γH2AX or NF-kB in green and IEA in red in presence of the vehicle ore the IL-6 receptor inhibitor Tocilizumab (TCZ). The infection was performed at MOI 1 and the analysis conducted 3 days post infection. The cells were marked with DAPI staining in blue. The panel showed the histogram analysis of the NF-kB/ γH2AX and IEA positive cells, vehicle TCZ, to quantify the reduction of paracrine damage in case of IL-6 receptor inhibition.*

4.5 IL-6 as a major player in the induction of paracrine senescence effect

The data obtained from immunofluorescence analyses shown in Figure 14 display effects of damage and inflammation in the neighbouring cells; furthermore, the presence of SASPs in supernatant from infected cells was investigated as the cause of this paracrine effect.

Considering the HCMV-infection supernatant characteristics, we asked if it was possible to provoke a senescent-phenotype like to new seeded cells. specifically, we infected RPTECs, HFF, and ARPE-19 cells and collected the supernatants at 3 days post infection. The

supernatant has been treated with UVB-light in order to inactivate any potential virion and analyse only the impact of SASP on the cells.

The conditioned media was used as treatment for 3 days. After these days, we performed an EdU incorporation staining in order to determine the cell proliferation ratio. It was possible to detect a significative reduction of cells only in RPTECs treated with UVB-infected supernatant compared to the mock counterpart (~ 35% *vs* 20%, respectively). Instead, we did not observe any EdU incorporation reduction in HFFs and ARPE-19 despite the conditioned media treatment.

To further validate the role of IL-6 in the paracrine senescence, we added TCZ to the conditioned media and then we treated fresh seeded RPTECs. We performed an EdU essay incorporation and in presence of TCZ we did not detect any variation in cell growth.

Next, we investigated the senescence as a host defence mechanism. To better understand this phenomenon, we collected 3 days post infection supernatants, then we treated RPTECs with those conditioned media and we simultaneously performed the infection. As shown in Figure 15F, RPTECs treated with "infected-conditioned media" (UVB-infected supernatant) are characterized by a reduction of IEA positive cells compared to "mock-conditioned media" (UVB-mock supernatant). Instead, if we replaced the conditioned media with fresh media, we could not observe any IEA positivity variation (Figure 15F). This further analysis was performed to see if there was an immediate impact of cytokines on virus entry into cells rather than longer-term on replication. The results obtained confirmed the interference of the SASP on the viral replication and the senescence as a host antiviral mechanism. We demonstrated a senescence phenotype in both infected RPTECs and HFFs, but we observed a paracrine senescence phenotype induced by IL-6 only in RPTECs.

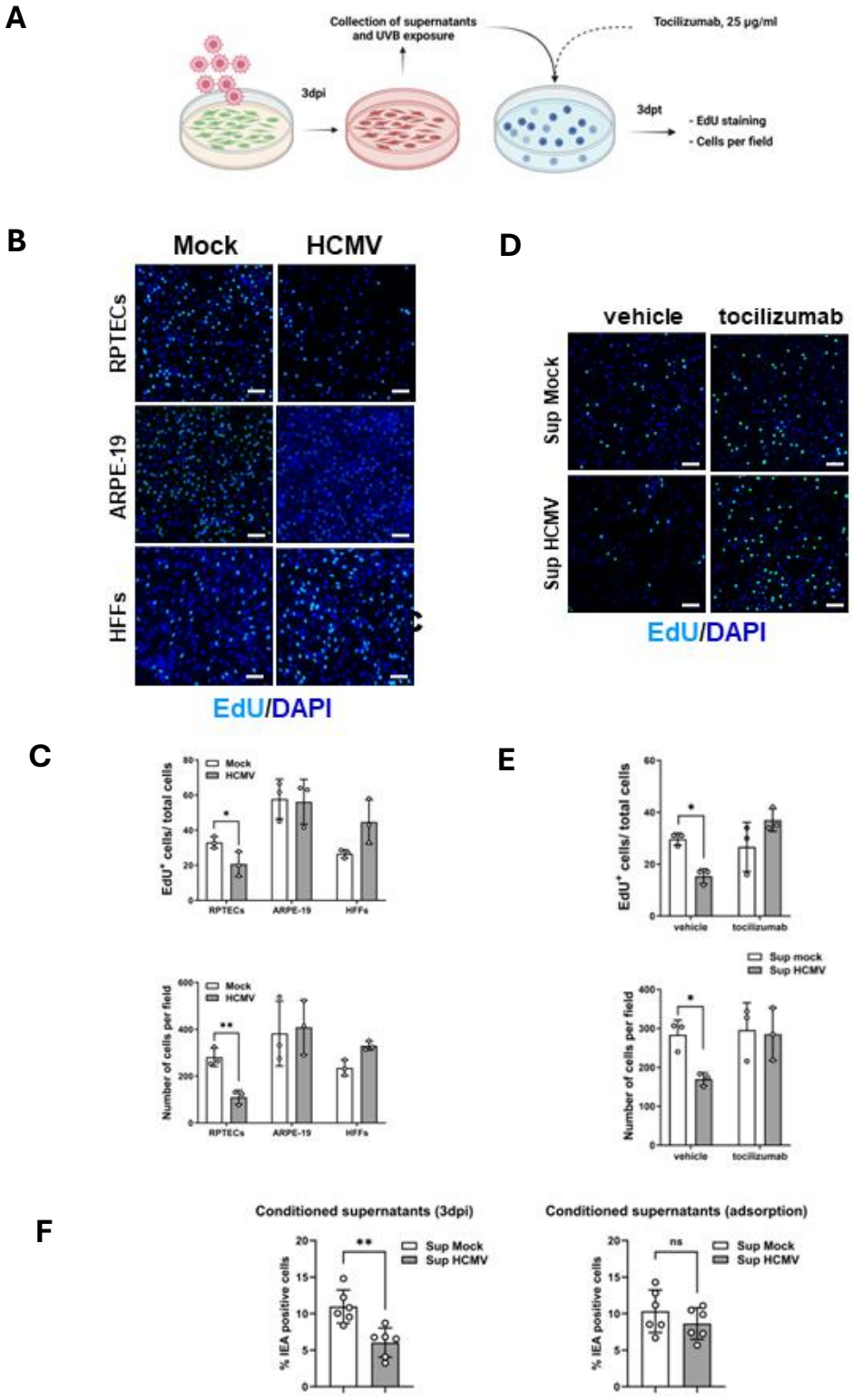

Figure 15. Demonstration of IL-6 dependent senescence upon HCMV infection in RPTECs. ***A***. *Schematic representation of the process followed to evaluate paracrine senescence in RPTECs, ARPE-19, and HFFs.* ***B***. *3 days post treatment, RPTECs, ARPE-19 cells and HFFs, with*

mock- and HCMV conditioned media, harvested after 3 days of infection at respectively MOI, were incubated with EdU for 20 h and stained as described in the Material and Methods section. DAPI was used to counterstain the nuclei. ***C.*** *These two graphs show respectively the percentage of EdU+ positive cells and the total number of cells among the three cell lines. D. Representative images of EdU incorporation staining in RPTECs of treated with conditioned media in the presence of TCZ (25 μg/mL) for 48h and then incubated with EdU for an additional 24 h, resulting in a total treatment period of 3 days.* ***E.*** *These two graphs show respectively the percentage of EdU+ positive cells and the total number of cells among the three cell lines in presence or not of TCZ.* ***F.*** *Representative graphs of IEA-positive infected RPTECS. The right one represents an infection performed with conditioned media for 3 days; the left one with conditioned media for the first 24 hours and then with the addition of fresh media for the last 2 days. The normalization exploit the number of DAPI-positive cells.*

4.6 Comparison between senescence induction by starvation and HCMV infection on RPTECs

We evaluated if senescence induced by starvation is comparable to the demonstrated VIS, in order to understand the behaviour of the fresh seeded cells when treated with starved media, such as a supernatant coming from a previous infection. This evaluation, as the previous one, was done on RPTECs because are the only characterized by the demonstrated VIS signature.

We seeded RPTECs and collected the supernatant after 5 days, and we used this starved media as treatment for fresh cells. We seeded RPTECs and treated them with this starved media for 3 days. At the end of the treatment, we evaluated the capability of the cells to proliferate and the presence of senescence markers. In particular, at 3 days post treatment we performed the EdU essay to evaluate the ability of cell proliferation. We used as control RPTECs grown in fresh media. We detected a significative ($P < 0.05$) reduction of EdU incorporation and of number of cells per field between starved media and control sample. Specifically, we measured 91% of EdU positive cell when RPTECs were grown in fresh media versus 39,4% of EdU positivity in cells treated with starved media. Then, we performed SA-β-gal assay to evaluate a second marker of senescence. We confirmed the previous data: the β-galactosidase activity was increased in starved media cells compared to the negative control; in particular we measured 59% SA-β-gal positive cells in fresh media treatment versus 80% in cells grown in starved media.

To thoroughly characterise senescence induced by starvation, we evaluated the mRNA regulation of two markers associated with senescence and proliferation. Specifically, we measured the mRNA expression levels of the proliferation marker Ki67 (*MKi67*) and of Lamin

B1 (*LAMINB1*) which is involved in chromatin changes and subsequently in senescence. We observed a significant decrease in *MKi67* expression after three days of treatment with starved media compared to fresh media. The same pattern of expression was maintained for *LAMINB1* mRNA levels.

Then, we used the same starved media added with Tocilizumab to understand if there was an involvement of IL-6. Despite of the presence of TCZ, the RPTECs treated with starved media decreased their proliferation and EdU incorporation (~ 25%; $P > 0.05$). This data highlighted the fact that the senescence-mechanism by starvation is not IL-6 dependant exclusively.

To conclude the characterization of the senescence induced by starvation and its effect, we evaluated the influence of this condition in case of infection. We infected RPTECs in presence of fresh media or starved media. The criteria of infections resemble the previous one: 3 days of infection at MOI 1. We performed an immunofluorescence to evaluate the expression of IEA as parameter of infection. Not surprisingly, based on the absence of the IL-6 effects in the induction of starvation-senescence, we did not detect any significative variation ($P > 0.05$) between these two conditions: the percentage of IEA positive cells was 22% versus 24%, respectively fresh versus starved media.

In conclusion, these experiments further emphasise that the induction of paracrine senescence adjacent to infection sites is an IL-6-dependent mechanism following active viral replication within the cell. In contrast, starvation-induced senescence, which along with oncogene-induced and virus-induced senescence is a characteristic phenomenon in our organism, is not attributable only to IL-6 but mostly to a mixture of factors without defensive mechanism against pathogens, while VIS is emerging as new type of senescence able to interfere with pathogens.

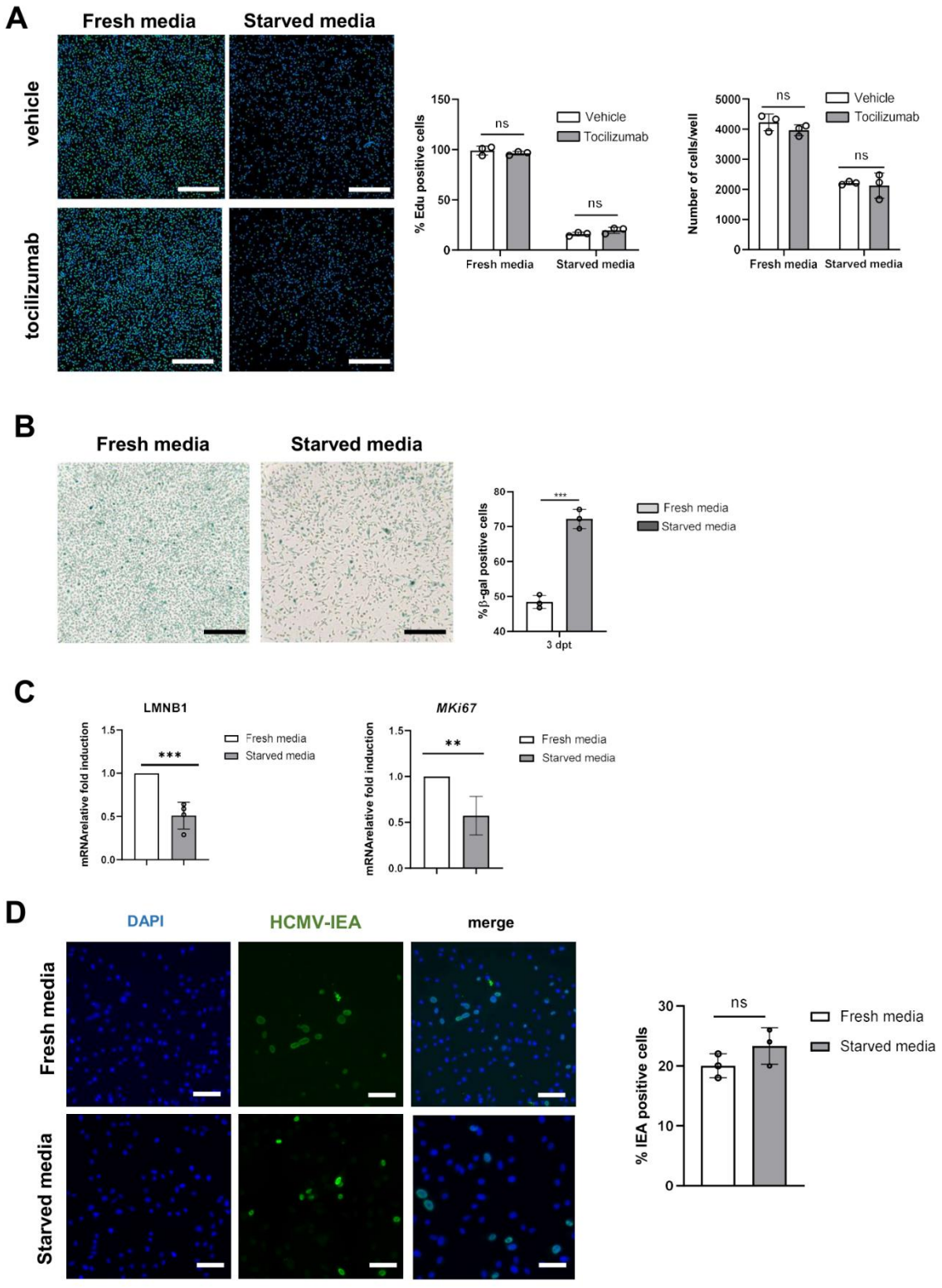

Figure 16. Characterization of senescence by starvation on RPTECS. ***A****. RPTECs: representative images and correlated graphs of EdU assay 3 days post treatment with fresh or starved media. The cells are counterstained with DAPI. RPTECs were incubated for 20 hours with EdU and*

stained as described in Material and methods. ***B****. Representative images of SA-β -gal staining of fresh- or starved-media treatment on RPTECs. The analysis has been performed 3 days post treatment, the SA-β -gal staining are the blue regions within the cells. The panel represents the percentage of SA-β-gal positive cells. There is a significative difference between fresh and starved media treatment.* ***C****. Quantitative PCR (qPCR) analysis was performed to measure mRNA expression levels of MKI67 and LAMINB1 from total RNA extracts collected at 3 days post-treatment with s fresh and starved media. Values were normalized to 18 S gene expression and presented as fold induction compared to fresh media-treated cells.* ***D****. Representative immunofluorescence of IEA in green and cells marked with DAPI staining in blue. The infection has been performed at MOI 1 and the analysis conducted 3 days post infection; fresh media versus starved media as condition of infection. The panel show the histogram analysis of the positive cells, fresh versus starved media, to quantify the difference percentage of IEA positive cells in the two conditions.*

5. DISCUSSION

In this research we highligh the fully replicative cycle of HCMV in our cell models and demonstrate the impact of the virus on the neighbouring uninfected cells. Specifically, we studied the secretory phenotype upon the infection and the main role of IL-6 in the induction of a senescence like-phenotype in RPTECs, that may play a role in the pathogenesis of kidney disease although it could also contribute to antiviral mechanisms. Firstly, we characterise the human cytomegalovirus infection in our model of interest, renal epithelial cells. In fact, we demonstrate the ability of HCMV to enter in all the three cell lines- RPTECs, HFFs and ARPE-19 cells, and to perform its replicative cycle. Our data demonstrate the production of the main three proteins involved in the functionality of the cytomegalovirus as well as the release of new virions, albeit to a lesser extent compared to virus-infected ARPE-19 cells.

Although, the infection of these three cells lines is quite similar, the evidence from the transcriptomic analysis reveals profound differences. HFFs and RPTECs share an Interferon-I response to HCMV infection that is not present in ARPE-19 cells. The GO-term shown in Figure 7A highlights an enrichment of the inflammatory response- characterized by cytokines such as IL-6, CXCL8, RANTES, CXCL10- in RPTECs but not in HFFs or ARPE-19 cells. Furthermore, epithelial renal cells are also enriched in the “hallmarks of rejection”, that is linkable to the in vivo evidence after kidney transplantation in human, while HFFs and ARPE-19 are missing in any hallmarks involved in organs damage. Of note, the unbalanced gene signature inflammatory response observed in RPTECs much resemble SASP[34]. Based on the evidence that SASP is suspected to be involved in in kidney fibrosis and rejection[39], we speculated that HCMV-infected RPTECs may exhibit features of VIS. To test our hypothesis, we first took advantage of the new established senescence-specific gene set SenMayo, and we found a significant enrichment of this senescence signature in HCMV-infected RPTECs and HFF but not in ARPE-19 cells. Second, we validate the presence of SASP by our Bio-Plex analysis, which reveals a massive release of inflammatory cytokines in the supernatants of infected RPTECs. In particular, TNF-α, IL-6, IL-8, and IL-9 are significantly upregulated at 1 dpi and remain elevated for up to 5 dpi, whereas GM-CSF, MIP1α, IP-10, PDGF-BB, and RANTES progressively increase overtime peaking at 5 dpi, with the sole exception of TNF-αD plateauing at 4 dpi. Finally, consistent with a picture of renal epithelial cell dysfunction, HCMV-infected RPTECs show increased expression and secretion of CXCL10/IP-10 and NGAL, known biomarkers of acute tubular injury and kidney graft rejection.

Moreover, earlier fibroblast in vitro research has demonstrated that viral infection alters the host cell cycle and causes cytoplasm expansion, replication stress induction, and the production of cytokines that promote inflammation. We previously described p53- and $p16^{INK4a}$-mediated early senescence in primary human cells infected with HCMV. Appropriately, the overexpression of the viral 86-kDa IE2 protein caused morphological alterations, such as the development of an expanded, flattened, and irregular shape—all typical characteristics of senescent cells—and elevated SA-β-gal production, inhibiting cellular DNA synthesis. These results therefore support the idea that HCMV infection might cause senescence in RPTECs, emphasizing the striking similarities in VIS programs seen in different cell types. It is in fact well-established that both DNA and RNA viruses can induce classic senescence hallmarks, such as SA-β-gal activity, increased expression of $p16^{INK4a}$, and $p21^{Waf1}$, as well as the secretion of pro-inflammatory SASP molecules, and the generation of reactive oxygen species (ROS).

However, defining a senescence profile unequivocally remains difficult due to the absence of a singular marker. In our model, we tried to establish a signature of virus-induced senescence exploiting some of the markers mentioned before. Specifically, when we analyzed the activity of β-galactosidase and the proliferation rate of HCMV-infected versus mock-infected cells, significant variations (increase SA-β-Gal activity and decrease in EdU incorporation) were noted in RPTECs and HFFs, but not in ARPE-19 cells. Furthermore, analysis of RNA expression levels for *LAMINB1* and *MKi67* highlighted important evidence of a senescence signature, with significant variations in RPTECs in HCMV-infected versus mock-infected cells. Moreover, our results indicated a much higher release of inflammatory cytokines, particularly IL-6 and IL-8, in RPTECs compared to HFFs and ARPE-19 cells. These findings pair the evidence derived from transcriptomic analysis, indicating that our model is characterized by a senescence signature upon infection. To conclude, our comprehensive analysis of these markers supports the presence of a senescence signature in virus-infected RPTECs, further corroborating the findings from our transcriptomic analysis.

Incontrovertible evidence that senescence is occurring in our cellular models comes from the high numbers of cells exhibiting nuclear positivity for NF-κB, γH2AX, and $p16^{INK4a}$, while lacking viral markers such as IE1. These findings indicate significant damage and senescence not only in infected cells but also in neighboring uninfected cells, a phenomenon unique limited to RPTECs, raising the possibility that virus-mediated paracrine senescence might be specific to renal tubular cells.

It is well established that a mixture of inflammatory cytokines released during infection can induce senescence, as demonstrated in the case of SARS-CoV-2 infection, and based on the results obtained so far we hypothesized that the inflammatory profile of the renal epithelial cells secretome can induce a paracrine senescence phenotype.

To further investigate the paracrine senescence phonotype in our model, we focused our experiment on IL-6, supported by Bio-Plex assay and transcriptomic analysis. Indeed, we observed a high release of IL-6 upon infection and an enrichment in the "IL-6/JAK-STAT3 signaling pathway" in HCMV-infected RPTECs. Tocilizumab (TCZ), a monoclonal antibody that binds to the IL-6 receptor and inhibits its activity, was used as treatment to evaluate if there is any variation in numbers of uninfected positive cells for NF-κB and γH2AX, two markers of senescence induction. As hypothesized, we measured a reduction in NF-κB and γH2AX in the nuclei of uninfected cells treated with TCZ, demonstrating IL-6's involvement in the paracrine senescence mechanism.

To further substantiate these results, we treated freshly seeded cells with UVB-inactivated conditioned media derived from previously infected cells. Renal epithelial cells treated with this conditioned media showed a significant reduction in EdU incorporation, indicating a decreased proliferation. However, this phenotype was reversed in the presence of TCZ. When the IL-6 receptor inhibitor was added to the UVB-inactivated media, cells resumed proliferation, suggesting that the conditioned medium's ability to trigger senescence in fresh cells is primarily mediated by factors such as IL-6, which can be neutralized by TCZ.

To conclude, we examined the role of this senescence signature during infection. HCMV infection was performed on RPTECs using UVB-inactivated conditioned media. We found no significant difference in IE1-positive cells between mock-conditioned media and infected-conditioned media when fresh media was used to stop the absorption after 24 hours. However, a significant variation was observed when the infection was performed with conditioned media for all the 3 days of infection, indicating that the different secretomes of these media play a role in the infectivity ability of the virus. This suggests that the senescence-associated secretory phenotype (SASP), particularly IL-6 in our model, released upon infection may have a protective role, inhibiting reinfection of the cells.

It is well known that an infection may result in an age-distorter event, characterized by a decrease of nutrients available for the cells and tissue, and that the decrease in nutritional factors within the infected HMCV-culture media may affect the capacity of the virus as well as the IL-

6 induction. To further confirm the dependence of the paracrine defensive mechanism based on IL-6 released upon infection, we characterized senescence due to starvation in RPTECs. Starvation-induced senescence was marked by increased β-galactosidase activity and reduced proliferation rate measured by EdU incorporation, similar to infection-induced senescence, as well as by a reduction of expression levels of *LAMINB1* and *MKi67*. However, adding TCZ to the starved media did not reverse the senescence phenotype, nor did it affect the infection results when using fresh or starved media. Indeed, the percentage of infected RPTECs showing a IEA positive immunofluorescence staining was comparable between fresh media Vs starved media and higher than the percentage of infected cells measured using infected HMCV-culture media. This indicates that in the case of starvation-induced senescence, the mechanism is not IL-6-dependent and underscores how nutrient deprivation can induce a phenotype resembling senescence RPTECs. However, this phenotype differs from that elicited during infection due to the absence of a pronounced inflammatory response (data not shown). Furthermore, this condition has a more significant impact than starvation alone on the virus's ability to initiate a lytic cycle in RPTECs.

Indirectly, we can speculate that senescence may be induced by various stimuli, and these stimuli may affect future cellular plasticity and responses to stressors, such as infections. This highlights the intricate interplay between cellular metabolic states and viral pathogenesis, suggesting avenues for further research into the modulation of cellular environments to influence disease outcomes. So, an important question raised by our results is whether HCMV gains an evolutionary advantage by driving cells into senescence. Although our findings do not clarify whether VIS favors viral persistent infection in growth-arrested but metabolically active epithelial cells, or if it is merely an incidental event that does not impact viral fitness, they provide the first evidence of a direct pathogenic mechanisms of HCMV infection in the kidney involving the induction of cellular senescence in a paracrine manner. Further research is clearly needed to fully understand the relevance of senescence in HCMV-mediated disease in vivo.

6. BIBLIOGRAPHY

1. McGeoch, D.J., Rixon, F.J., and Davison, A.J. (2006). Topics in herpesvirus genomics and evolution. Virus Research *117*, 90–104. https://doi.org/10.1016/j.virusres.2006.01.002.

2. Dioverti, M.V., and Razonable, R.R. (2016). Cytomegalovirus. Microbiol Spectr *4*, 4.4.20. https://doi.org/10.1128/microbiolspec.DMIH2-0022-2015.

3. Griffiths, P., and Reeves, M. (2021). Pathogenesis of human cytomegalovirus in the immunocompromised host. Nat Rev Microbiol *19*, 759–773. https://doi.org/10.1038/s41579-021-00582-z.

4. Pesch, M.H., Kuboushek, K., McKee, M.M., Thorne, M.C., and Weinberg, J.B. (2021). Congenital cytomegalovirus infection. BMJ, n1212. https://doi.org/10.1136/bmj.n1212.

5. Plosa, E.J., Esbenshade, J.C., Fuller, M.P., and Weitkamp, J.-H. (2012). Cytomegalovirus Infection. Pediatrics In Review *33*, 156–163. https://doi.org/10.1542/pir.33.4.156.

6. Butcher, S.J., Aitken, J., Mitchell, J., Gowen, B., and Dargan, D.J. (1998). Structure of the Human Cytomegalovirus B Capsid by Electron Cryomicroscopy and Image Reconstruction. Journal of Structural Biology *124*, 70–76. https://doi.org/10.1006/jsbi.1998.4055.

7. Foglierini, M., Marcandalli, J., and Perez, L. (2019). HCMV Envelope Glycoprotein Diversity Demystified. Front. Microbiol. *10*, 1005. https://doi.org/10.3389/fmicb.2019.01005.

8. Kalejta, R.F. (2008). Tegument Proteins of Human Cytomegalovirus. Microbiol Mol Biol Rev *72*, 249–265. https://doi.org/10.1128/MMBR.00040-07.

9. Biolatti, M., Dell'Oste, V., Andrea, M.D., and Landolfo, S. The human cytomegalovirus tegument protein pp65 (pUL83): a key player in innate immune evasion.

10. Connolly, S.A., Jardetzky, T.S., and Longnecker, R. (2021). The structural basis of herpesvirus entry. Nat Rev Microbiol *19*, 110–121. https://doi.org/10.1038/s41579-020-00448-w.

11. Nguyen, C.C., and Kamil, J.P. (2018). Pathogen at the Gates: Human Cytomegalovirus Entry and Cell Tropism. Viruses *10*, 704. https://doi.org/10.3390/v10120704.

12. Compton, T., Nepomuceno, R.R., and Nowlin, D.M. (1992). Human cytomegalovirus penetrates host cells by PH-independent fusion at the cell surface. Virology *191*, 387–395. https://doi.org/10.1016/0042-6822(92)90200-9.

13. Forte, E., Zhang, Z., Thorp, E.B., and Hummel, M. (2020). Cytomegalovirus Latency and Reactivation: An Intricate Interplay With the Host Immune Response. Front. Cell. Infect. Microbiol. *10*, 130. https://doi.org/10.3389/fcimb.2020.00130.

14. Kuny, C.V., and Kalejta, R.F. (2016). Human Cytomegalovirus Can Procure Deoxyribonucleotides for Viral DNA Replication in the Absence of Retinoblastoma Protein Phosphorylation. J Virol *90*, 8634–8643. https://doi.org/10.1128/JVI.00731-16.

15. Turner, D.L., and Mathias, R.A. (2022). The human cytomegalovirus decathlon: Ten critical replication events provide opportunities for restriction. Front. Cell Dev. Biol. *10*, 1053139. https://doi.org/10.3389/fcell.2022.1053139.

16. Poole, E., Lau, J., Groves, I., Roche, K., Murphy, E., Carlan Da Silva, M., Reeves, M., and Sinclair, J. (2023). The Human Cytomegalovirus Latency-Associated Gene Product Latency Unique Natural Antigen Regulates Latent Gene Expression. Viruses *15*, 1875. https://doi.org/10.3390/v15091875.

17. Gerna, G., Kabanova, A., and Lilleri, D. (2019). Human Cytomegalovirus Cell Tropism and Host Cell Receptors. Vaccines *7*, 70. https://doi.org/10.3390/vaccines7030070.

18. Grossi, P.A., Kamar, N., Saliba, F., Baldanti, F., Aguado, J.M., Gottlieb, J., Banas, B., and Potena, L. (2022). Cytomegalovirus Management in Solid Organ Transplant Recipients: A Pre-COVID-19 Survey From the Working Group of the European Society for Organ Transplantation. Transpl Int *35*, 10332. https://doi.org/10.3389/ti.2022.10332.

19. De Keyzer, K., Van Laecke, S., Peeters, P., and Vanholder, R. (2011). Human Cytomegalovirus and Kidney Transplantation: A Clinician's Update. American Journal of Kidney Diseases *58*, 118–126. https://doi.org/10.1053/j.ajkd.2011.04.010.

20. Gorgoulis, V., Adams, P.D., Alimonti, A., Bennett, D.C., Bischof, O., Bishop, C., Campisi, J., Collado, M., Evangelou, K., Ferbeyre, G., et al. (2019). Cellular Senescence: Defining a Path Forward. Cell *179*, 813–827. https://doi.org/10.1016/j.cell.2019.10.005.

21. McHugh, D., and Gil, J. (2018). Senescence and aging: Causes, consequences, and therapeutic avenues. Journal of Cell Biology *217*, 65–77. https://doi.org/10.1083/jcb.201708092.

22. Chou, J.P., and Effros, R.B. (2013). T CELL REPLICATIVE SENESCENCE IN HUMAN AGING.

23. Zhu, H., Blake, S., Kusuma, F.K., Pearson, R.B., Kang, J., and Chan, K.T. (2020). Oncogene-induced senescence: From biology to therapy. Mechanisms of Ageing and Development *187*, 111229. https://doi.org/10.1016/j.mad.2020.111229.

24. Shvedova, M., Samdavid Thanapaul, R.J.R., Thompson, E.L., Niedernhofer, L.J., and Roh, D.S. (2022). Cellular Senescence in Aging, Tissue Repair, and Regeneration. Plastic & Reconstructive Surgery *150*, 4S-11S. https://doi.org/10.1097/PRS.0000000000009667.

25. Kumari, R., and Jat, P. (2021). Mechanisms of Cellular Senescence: Cell Cycle Arrest and Senescence Associated Secretory Phenotype. Front. Cell Dev. Biol. *9*, 645593. https://doi.org/10.3389/fcell.2021.645593.

26. Ogrodnik, M., Salmonowicz, H., and Gladyshev, V.N. (2019). Integrating cellular senescence with the concept of damage accumulation in aging: Relevance for clearance of senescent cells. Aging Cell *18*, e12841. https://doi.org/10.1111/acel.12841.

27. James, E.L., Michalek, R.D., Pitiyage, G.N., De Castro, A.M., Vignola, K.S., Jones, J., Mohney, R.P., Karoly, E.D., Prime, S.S., and Parkinson, E.K. (2015). Senescent Human Fibroblasts Show Increased Glycolysis and Redox Homeostasis with Extracellular Metabolomes That Overlap with Those of Irreparable DNA Damage, Aging, and Disease. J. Proteome Res. *14*, 1854–1871. https://doi.org/10.1021/pr501221g.

28. Rovira, M., Sereda, R., Pladevall-Morera, D., Ramponi, V., Marin, I., Maus, M., Madrigal-Matute, J., Díaz, A., García, F., Muñoz, J., et al. (2022). The lysosomal proteome of senescent cells contributes to the senescence secretome. Aging Cell *21*, e13707. https://doi.org/10.1111/acel.13707.

29. Bernadotte, A., Mikhelson, V.M., and Spivak, I.M. (2016). Markers of cellular senescence. Telomere shortening as a marker of cellular senescence. Aging *8*, 3–11. https://doi.org/10.18632/aging.100871.

30. Martínez, I., García-Carpizo, V., Guijarro, T., García-Gomez, A., Navarro, D., Aranda, A., and Zambrano, A. (2016). Induction of DNA double-strand breaks and cellular senescence by human respiratory syncytial virus. Virulence *7*, 427–442. https://doi.org/10.1080/21505594.2016.1144001.

31. Wiley, C.D., and Campisi, J. (2016). From Ancient Pathways to Aging Cells—Connecting Metabolism and Cellular Senescence. Cell Metabolism *23*, 1013–1021. https://doi.org/10.1016/j.cmet.2016.05.010.

32. Docherty, M.-H., O'Sullivan, E.D., Bonventre, J.V., and Ferenbach, D.A. (2019). Cellular Senescence in the Kidney. JASN *30*, 726–736. https://doi.org/10.1681/ASN.2018121251.

33. Docherty, M.H., Baird, D.P., Hughes, J., and Ferenbach, D.A. (2020). Cellular Senescence and Senotherapies in the Kidney: Current Evidence and Future Directions. Front. Pharmacol. *11*, 755. https://doi.org/10.3389/fphar.2020.00755.

34. Cuollo, L., Antonangeli, F., Santoni, A., and Soriani, A. (2020). The Senescence-Associated Secretory Phenotype (SASP) in the Challenging Future of Cancer Therapy and Age-Related Diseases. Biology *9*, 485. https://doi.org/10.3390/biology9120485.

35. Nogalski, M.T., Solovyov, A., Kulkarni, A.S., Desai, N., Oberstein, A., Levine, A.J., Ting, D.T., Shenk, T., and Greenbaum, B.D. (2019). A tumor-specific endogenous repetitive element is induced by herpesviruses. Nat Commun *10*, 90. https://doi.org/10.1038/s41467-018-07944-x.

36. Kojima, H., Inoue, T., Kunimoto, H., and Nakajima, K. (2013). IL-6-STAT3 signaling and premature senescence. JAK-STAT *2*, e25763. https://doi.org/10.4161/jkst.25763.

37. Field, M., Lowe, D., Cobbold, M., Higgins, R., Briggs, D., Inston, N., and Ready, A.R. (2014). The use of NGAL and IP-10 in the prediction of early acute rejection in highly sensitized patients following HLA-incompatible renal transplantation. Transpl Int *27*, 362–370. https://doi.org/10.1111/tri.12266.

38. Michelson, S., Dal Monte, P., Zipeto, D., Bodaghi, B., Laurent, L., Oberlin, E., Arenzana-Seisdedos, F., Virelizier, J.L., and Landini, M.P. (1997). Modulation of RANTES

production by human cytomegalovirus infection of fibroblasts. J Virol *71*, 6495–6500. https://doi.org/10.1128/jvi.71.9.6495-6500.1997.

39. Sosa Peña, M.D.P., Lopez-Soler, R., and Melendez, J.A. (2018). Senescence in chronic allograft nephropathy. American Journal of Physiology-Renal Physiology *315*, F880–F889. https://doi.org/10.1152/ajprenal.00195.2016.